Polyanionic-based cathode materials for K-ion batteries

Gwangeon Oh [a,1], Hyokyeong Kang [a,1], Hyeona Park [a,1], Heesung Shin [a], Seungwon Lee [a], Changki Jeon [a], Shizhao Xiong [b], Dominic Bresser [c,d], Jian Wang [b,*], Jang-Yeon Hwang [a,e,*]

[a] Department of Energy Engineering, Hanyang University, Seoul 04763, Republic of Korea
[b] Faculty of Material Science and Engineering, Kunming University of Science and Technology, Kunming, 650093, China
[c] Helmholtz Institute Ulm (HIU), Helmholtzstrasse 11, 89081 Ulm, Germany
[d] Karlsruhe Institute of Technology (KIT), P.O. Box 3640, 76021 Karlsruhe, Germany
[e] Department of Battery Engineering, Hanyang University, Seoul 04763, Republic of Korea

Keywords:
K-ion batteries
Polyanionic frameworks
Cathode
High-voltage
Strong covalent bond

A B S T R A C T

The urgent need for sustainable energy storage solutions beyond lithium-ion batteries (LIBs) has propelled K-ion batteries (KIBs) into the spotlight, leveraging potassium's crustal abundance, cost-effectiveness, and favorable ionic mobility. This review critically examines the transformative potential of polyanionic cathode materials in addressing the unique challenges posed by K^+ ions notably their large ionic radius (1.38 Å) and structural compatibility while capitalizing on their high-voltage operation and robust cycling stability. We elucidate the structural and electrochemical merits of polyanionic frameworks (e.g., phosphate, fluorophosphate, sulfates, and pyrophosphate), emphasizing their capacity to stabilize high-voltage operation (>4.0 V vs. K/K^+) through inductive effects enabled by strong covalent X–O bonds (*X* *P*, S, F). Key material families, including NASICON-type $K_3V_2(PO_4)_3$, fluorosulfate ($KFeSO_4F$), and mixed polyanion systems ($K_4Fe_3(PO_4)_2P_2O_7$), are systematically analyzed to unravel structure-property-performance relationships. Advanced synthesis strategies such as sol-gel processing, hydrothermal templating, and electrochemical ion exchange are highlighted for their role in optimizing ionic/electronic conductivity and mitigating interfacial instability. Despite progress, challenges persist in balancing energy density (>400 Wh kg^{-1} calculated based on the cathode mass) with cyclability (>1000 cycles), necessitating synergistic strategies like nanoscale engineering, anion/cation co-doping, and conductive matrix integration. The review underscores the untapped potential of titanium- and manganese-based polyanionics, metastable fluorophosphate derivatives, and hierarchical architectures to overcome kinetic limitations. By bridging fundamental insights with scalable manufacturing considerations, this work provides a roadmap for advancing KIBs toward grid-scale storage and electrified transportation, circumventing lithium's geopolitical constraints while unlocking new frontiers in high-energy, sustainable electrochemistry.

1. Introduction

With the world's acute environmental issue like air pollution and oil depletion, the demand for renewable energy is increasing [1,2]. While wind and solar energy are pivotal to decarbonization efforts, their inherent intermittency and transient output necessitate reliable energy storage solutions to mitigate energy wastage and stabilize grid supply [3]. Among existing technologies, lithium-ion batteries (LIBs) dominate the rechargeable battery market due to their high energy density, power efficiency, and established commercialization pathways [4]. Originally confined to portable electronics, LIBs now underpin large-scale applications such as electric vehicles (EVs) and grid-scale energy storage systems (ESS), driving unprecedented demand for lithium resources.

Lithium's scarcity (constituting merely ~0.002–0.0065 % of Earth's crust) and geopolitical concentration pose severe supply chain vulnerabilities, exacerbating price volatility and long-term resource insecurity [5], a critical bottleneck that has spurred research into alternative rechargeable battery chemistries. Among these, KIBs have emerged as a particularly promising candidate, primarily due to potassium's significantly higher crustal abundance (~2.6 %) and the lower cost of its raw materials (e.g., K_2CO_3 at ~$1100–1500/tonne compared to Li_2CO_3 at ~$9000–11,000/tonne, even at recent lows) [6]. Further bolstering their

* Corresponding authors.
E-mail addresses: wangjian96ld@163.com (J. Wang), jangyeonhw@hanyang.ac.kr (J.-Y. Hwang).
[1] These authors contributed equally to this work.

potential, KIBs offer electrochemical similarities to lithium, compatibility with the existing graphite anode supply chain, and the ability to utilize more economical aluminum current collectors for both anode and cathode. This presents cost and processing benefits compared to Na-ion batteries (NIBs), which often require specialized hard carbon anodes, and LIBs, which use more expensive copper for the anode current collector. Recent advancements highlight KIBs' potential, with practical full-cell gravimetric energy densities reaching approximately 100–173 Wh/kg and a target of 150–180 Wh/kg comparable to commercial lithium iron phosphate (LFP) batteries coupled with seamless integration possibilities with existing manufacturing infrastructure [7,8]. Concurrently, their operating voltage, typically ~3.0–4.1 V with some systems potentially reaching 4.5 V, is competitive, often exceeding that of NIBs and approaching that of LIBs [9,10]. Although further improvements are necessary for KIBs concerning volumetric energy density, cycle life, and comprehensive full-cell safety data, their pronounced cost and resource advantages, combined with ongoing technological progress, provide a strong rationale for continued investment in KIB research towards next-generation energy storage solutions.

The advancement of KIB technology hinges critically on reconciling the inherent physicochemical properties of K^+ ions with the structural adaptability of cathode materials [11]. Among alkali ions, K^+ exhibits a smaller Stokes radius (2.32 Å) compared to Li^+ (2.37 Å) and Na^+ (2.76 Å) in PC based electrolyte, owing to its weaker Lewis acidity [12]. This property enables superior ionic mobility, higher transference numbers (0.8–0.9 vs. 0.2–0.4 for Li^+), and reduced desolvation energy barriers (~0.7 eV vs. ~1.0 eV for Li^+), theoretically favoring fast charge transfer kinetics [13]. However, the larger ionic radius of K^+ (1.38 Å) compared to Li^+ (0.76 Å) and Na^+ (1.02 Å) imposes critical challenges in developing cathode frameworks that enable the reversible K^+ (de)insertion without structural collapse (Fig. 1**a**) [14]. Finally, K metal exhibits a significantly lower shear modulus (1.3 GPa) compared to Na (3.3 GPa) and Li (4.1 GPa), which facilitates the formation of smooth K-metal anodes after mechanical cutting [15]. This intrinsic smoothness of potassium metal contributes to a more uniform plating/stripping process, thereby enhancing its practical applicability as an anode material in potassium-based batteries (Fig. 1**a**) [15].However, the negative potential value of $E^o(K^+/K)$, compared to $E^o(Li^+/Li)$, $E^o(Na^+/Na)$, indicating a lower potential boundary for KIB negative electrodes compared to those in LIBs and NIBs, thereby KIBs achieve the widest voltage window (4.6 V) compared to the respective 4.5 and 4.2 V of Li and Na systems (Fig. 1**b**) [16]. To use KIBs while utilizing their advantages, it is crucial to enhance the operating voltage by designing the appropriate anode while preventing potassium deposition (Fig. 1**c**) [17].

To address this dichotomy, three cathode archetypes have emerged as frontrunners for KIBs: i) Layered/spinel oxides (e.g., K_xMO_2), leveraging their high theoretical capacities (120–200 mAh g^{-1}) and compatibility with existing LIB manufacturing infrastructure. Their open 2D diffusion channels mitigate K^+ migration barriers, though Jahn-Teller distortions and phase transitions during deep cycling remain challenges [18]. ii) Prussian blue analogues (PBAs) ($A_xM[Fe(CN)_6]$ $y{\cdot}nH_2O$), where their 3D open framework (≈5 Å interstitial sites) enables rapid K^+ diffusion and exceptional cyclability (>5000 cycles) [19]. iii) Polyanion compounds (e.g., $KVPO_4F$), utilizing strong X-O ($X = P$, S, B) covalent bonding to stabilize high-voltage operation (>4 V vs. K/K^+). The inductive effect of PO_4^{3-} groups in $K_3V_2(PO_4)_3$ enables a 3.7 V plateau and 93 % capacity retention after 200 cycles [20].

Fig. 2 demonstrated the comparison of cycle life, specific capacity, average voltage, tap density, safety, and economic feasibility of various cathode materials including polyanionic compounds, layered oxides,

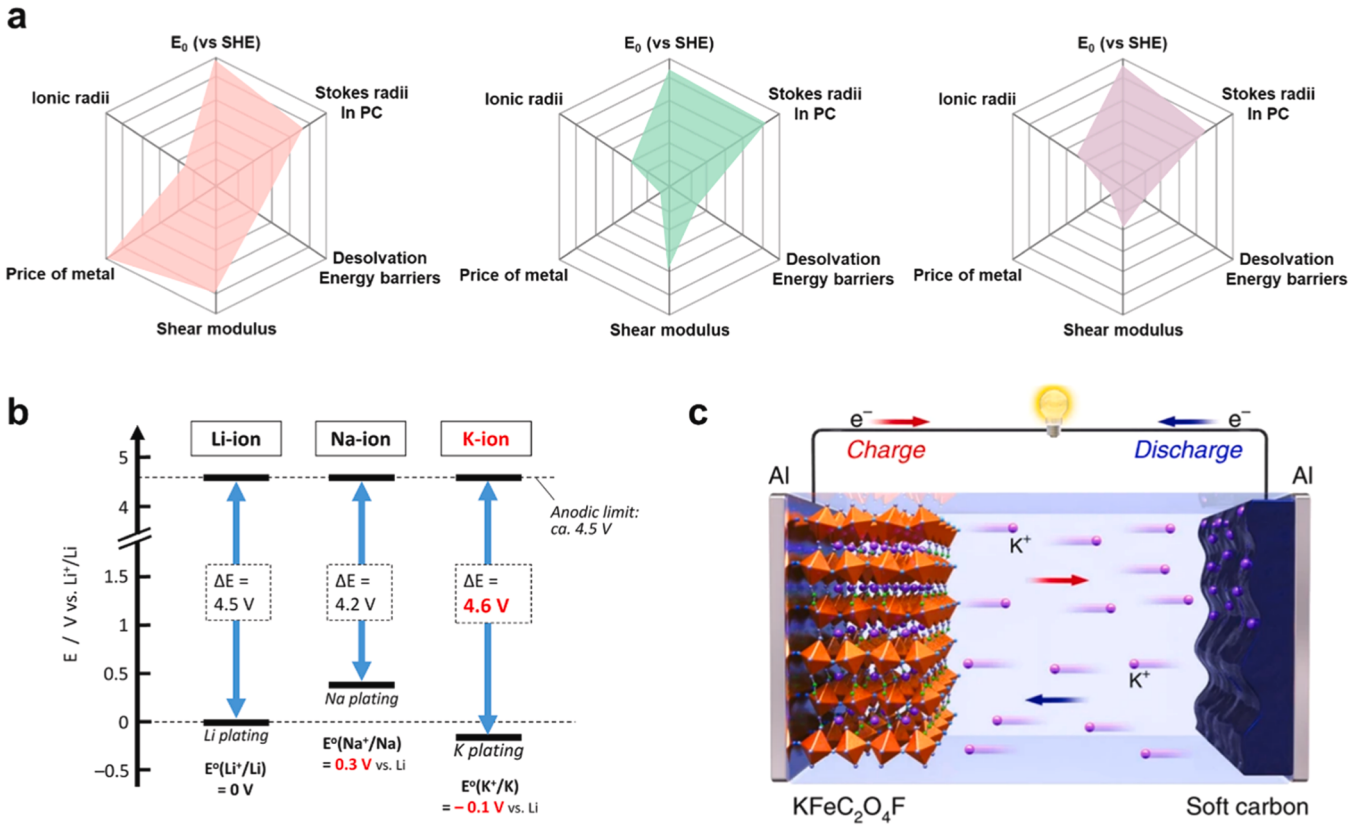

Fig. 1. (a) Properties of Li^+, Na^+, and K^+ as charge carriers for rocking-chair batteries and the price of the corresponding metals. (b) Available potential windows of Li^+, Na^+, and K^+ based batteries assuming nonaqueous electrolytes with carbonate ester solvents. Reproduced with permission [16] Copyright 2020, American Chemical Society. All rights reserved. (c) Schematic diagram of potassium ion batteries. Reproduced with permission [17] Copyright 2020, The Author(s). All rights reserved.

and Prussian blue analogues for KIBs using spider maps. Polyanionic compounds exhibit lower tap density than layered oxides. This is primarily because the inherently low ionic conductivity of polyanionic materials necessitates particle downsizing to the nanoscale, which consequently reduces the tap density [21]. In terms of specific capacity, unlike Na-ion battery systems where considerable variation exists among cathode materials, K-ion battery cathodes including polyanionic, layered, and Prussian blue-based materials tend to exhibit similar capacity levels [16]. Polyanionic compounds demonstrate higher average voltage, longer cycle life, and enhanced safety characteristics compared to other cathode types. These advantages largely stem from their intrinsic structural features. Polyanion-type materials generally adopt a chemical formula of $K_xM_y(XO_4)_n$ ($X = S$, P, or F; M = transition metal), where the tetrahedral anionic units $(XO_4)^{n-}$ or their derivatives $(X_mO_{3m+1})^{n-}$ form strong covalent bonds with MO_x polyhedral [22]. The presence of strong X–O covalent interactions leads to highly localized valence electrons, which in turn stabilizes high redox potentials of the transition metals. Moreover, the robust 3D frameworks of these compounds minimize structural distortion during K^+ intercalation/deintercalation, enabling stable high-voltage redox reactions (>4.0 V vs. K/K^+) [23]. These structural characteristics contribute significantly to the superior voltage output, cycling stability, and inherent safety of polyanionic cathodes. Lastly, polyanionic compounds also offer reasonable economic advantages. Their synthesis processes are compatible with those established for lithium iron phosphate ($LiFePO_4$) and sodium polyanionic cathodes, enabling cost-effective scale-up [1]. While several studies have focused on vanadium-based systems, polyanionic cathodes can be synthesized using earth-abundant, non-toxic, and inexpensive elements such as potassium, iron, manganese, and phosphorus, avoiding reliance on costly and less sustainable transition metals like nickel and cobalt [24] (Table 1).

Despite the promising attributes of polyanionic compounds, including their structural robustness, tunable redox potentials, and enhanced thermal stability their full potential in KIBs remains underexplored compared to mature Li/Na-ion systems. The unique interplay between strongly covalent polyanion frameworks (e.g., PO_4^{3-}, SO_4^{2-}) and K^+ ion dynamics offers unparalleled opportunities to address critical challenges in high-energy-density storage, such as mitigating Jahn-Teller distortions and suppressing transition metal dissolution. However, key obstacles persist, including low intrinsic electronic conductivity, sluggish K^+ diffusion kinetics in rigid frameworks, and interfacial incompatibility with conventional electrolytes. This review systematically examines the latest advances in polyanionic cathode design for KIBs, spanning crystallographic engineering, anion/cation co-doping strategies, and nanostructural optimization to enhance both energy density (>400 Wh kg^{-1}) and cycle life (>1000 cycles). By critically analyzing structure-property-performance relationships across phosphate, sulfate, fluorophosphate, and mixed-polyanion families, we identify design principles for balancing high-voltage operation (>4.0 V vs. K/K^+) with structural resilience. Furthermore, we evaluate scalable synthesis routes and compatibility with anode/electrolyte systems to bridge the gap between laboratory breakthroughs and commercial viability. This work aims to establish a roadmap for next-generation KIBs, emphasizing how polyanionic cathodes could unlock grid-scale energy storage and electrified transportation markets while circumventing lithium's geopolitical constraints.

2. Review on potassium based polyanionic compounds

2.1. Structural features

The operating voltage of a battery is a key determinant of its energy density, and in polyanionic cathodes, this voltage is significantly influenced by a phenomenon known as the "inductive effect". Potassium-based polyanionic compounds, typically represented by the general formula $K_x(TM)_z(XO_4)_m^n$ (where TM = transition metal; $X = B$, P, Si, S, Mo, As, Ti, V), constitute an underexplored class of cathode materials for KIBs [25,26]. X can regulate the electronic environment of the redox-active TM center. This regulation in turn determines the energy of the TM redox couple and thus the operating voltage of the battery. Three distinct structural configurations dominate polyanionic compounds: (i) Mixed polyanion units with shared X centers (e.g., $(PO_4)^{3-}$–$(P_2O_7)^{4-}$, $(SO_4)^{2-}$–$(S_2O_3)^{2-}$), which enable lattice flexibility and ion diffusion pathways (Fig. 3a) [27]. (ii) Hybrid anion systems combining oxyanions with monovalent anions (e.g., $(PO_4)^{3-}$–F^-), where fluorine substitution enhances structural stability and ionic conductivity (Fig. 3**b**) [28]. (iii) Dual oxyanion frameworks (e.g., $(PO_4)^{3-}$–$(SO_4)^{2-}$, $(C_2O_4)^{2-}$–$(SO_4)^{2-}$), which synergistically modulate redox potentials and ion mobility (Fig. 3**c**) [29].

The inductive effect in polyanionic cathode materials originates from the high electronegativity of the central atom X within the $(XO_4)^n$ polyanion or of substituent atoms like fluorine [30,31]. This pronounced electronegativity enhances the covalent character of X-O bonds. Consequently, oxygen atoms coordinating the TM exhibit reduced electron-donating capability, thereby increasing the ionicity of the TM-O bonds [32]. This alteration, or the direct M-F interaction, effectively lowers the energy levels of the TM d-electrons relative to the anode's Fermi level [33]. As a result, a greater energy input is required for TM oxidation, or more energy is released during TM reduction, culminating in an elevated overall cell voltage. This phenomenon, underpinned by the intrinsic stability of the polyanionic framework, describes how strong electronegative groups modulate TM redox potentials by dispersing electron density around TM-O bonds, thereby increasing ionization energy and raising cationic redox voltages.

The selection of the central atom X within $(XO_4)^n$ polyanions, primarily phosphorus or sulfur, critically dictates the inductive effect's magnitude and thereby the TM's redox potential [30]. Phosphate ($(PO_4)^{3-}$) groups, characterized by phosphorus's electronegativity (Pauling scale ~2.19) and strong covalent P-O bonds, effectively withdraw electron density from oxygen atoms coordinating the TM, enhancing TM-O bond ionicity and elevating redox potentials compared to simple oxides. Pyrophosphate ($(P_2O_7)^{4-}$) units, with a higher

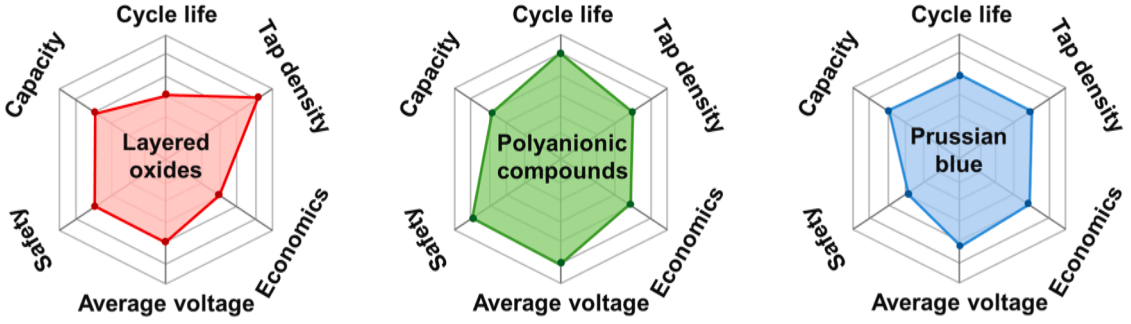

Fig. 2. Key properties of layered oxide, polyanionic compounds, and Prussian blue analogs cathode material for KIBs.

Table 1
Key technoeconomic and performance metrics for KIBs, NIBs, and LIBs.

Feature	KIBs	NIBs	LIBs
Practical Energy Density (Gravimetric)	~100–173 Wh/kg (prototypes); Target: 150–180 Wh/kg	~75–160 Wh/kg (commercial/prototypes); some lab cells higher	LFP: 90–160 Wh/kg; NMC: 150–250 Wh/kg; High-end: up to 360 Wh/kg
Practical Energy Density (Volumetric)	Data limited	~250–375 Wh/L	LFP: 300–350 Wh/L; NMC: 500–700 Wh/L
Average Cell Voltage	~3.0–4.1 V (prototypes); potential up to 4.5 V	~3.0–3.2 V; some systems 1.0–4.2 V	LFP: ~3.2 V; NMC: ~3.6–3.7 V
Cycle Life	700–2000+ cycles (prototypes)	Highly variable (few 100 s to >4000 cycles, e.g., Natron)	LFP: 2500–5000+ cycles; NMC: 500–2000 cycles
Raw Material Abundance	K: ~2.6 % (High)	Na: ~2.4–2.8 % (Very High)	Li: ~0.002–0.0065 % (Low)
Raw Material Cost	K_2CO_3: ~$1100–1500/tonne	Na_2CO_3: ~$230–360/tonne	Li_2CO_3: ~$9000–11,000/tonne
Safety	Polyanion materials offer good thermal stability; Full-cell data limited.	Generally good; Al current collectors; 0 V storage. Some concerns with hard carbon anodes & thermal runaway.	Mature BMS required; Flammable organic electrolytes are a concern.
Key Advantages	Abundant K, low cost, graphite anode compatibility, high voltage potential, Al current collectors.	Very abundant Na, lowest raw material cost, Al current collectors, improving performance.	Highest energy density, mature technology, established supply chain.
Key Challenges	Lower practical energy density than LIBs currently, larger K^+ ion challenges electrode structure/kinetics, limited Wh/L & full-cell safety data.	Lower energy density than LIBs, larger Na^+ ion, cycle life can vary, anode material optimization.	Cost, Li resource constraints, safety concerns, reliance on critical materials (Co, Ni).
Primary Anode	Graphite, other carbons	Hard Carbon, other carbons, some alloys	Graphite, Si-composites
Current Collectors	Aluminum (Anode & Cathode)	Aluminum (Anode & Cathode)	Copper (Anode), Aluminum (Cathode)

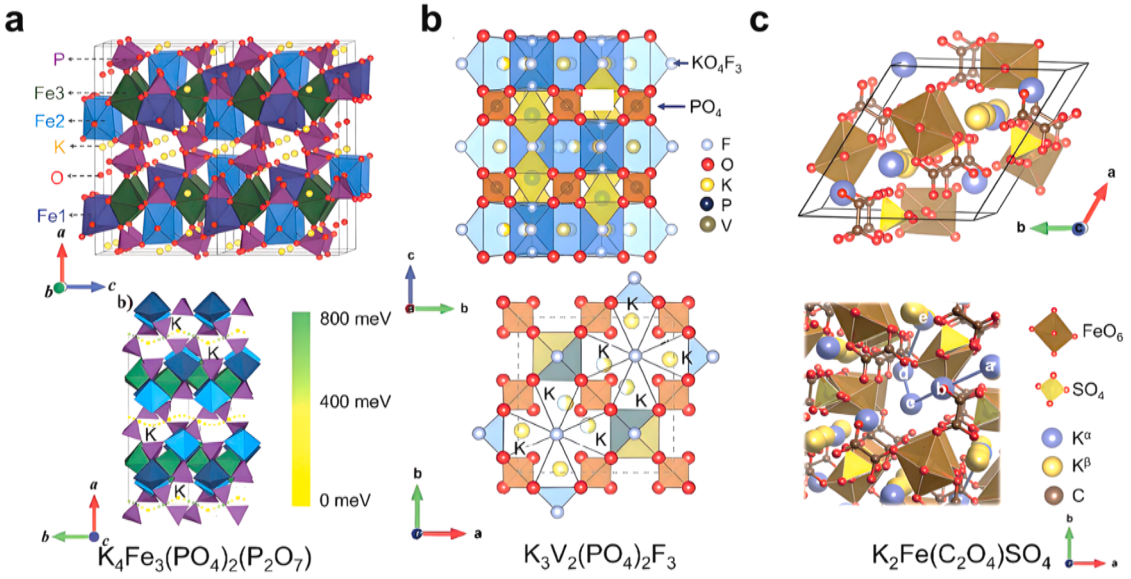

Fig. 3. Schematic crystal structure of (a) $K_4Fe_3(PO_4)_2(P_2O_7)$ [27]. (b) $K_3V_2(PO_4)_2F_3$ [28]. (c) $K_2Fe(C_2O_4)SO_4$ [29].

concentration of electronegative phosphorus, generally exhibit a more potent inductive effect and thus yield higher TM redox potentials than orthophosphates, albeit sometimes at the expense of thermal stability [34]. This increased ionicity in TM-O bonds, induced by either phosphate variant, stabilizes TM d-electron energy levels, directly contributing to increased cell operating voltages.

Sulfur (Pauling electronegativity ~2.58), being notably more electronegative than phosphorus, forms more covalent and stronger S-O bonds within sulfate ($(SO_4)^2$) groups. This results in a significantly more pronounced inductive effect, leading to a greater increase in TM-O bond ionicity and a more substantial elevation of the TM redox potential relative to phosphate-based analogues, establishing an inductive strength hierarchy of $(SO_4)^2$ > $(P_2O_7)^4$ > $(PO_4)^3$ [35]. While sulfate-containing materials can achieve superior operating voltages, they often present challenges such as limited thermal stability (typically below 400 °C) and potential solubility in aqueous electrolytes, which can restrict their practical application [36]. Therefore, while the choice of polyanion is a key strategy for tuning redox potentials, the pursuit of higher voltages through stronger inductive effects necessitates careful consideration of material stability, synthetic viability, and overall performance trade-offs.

Fluorine incorporation into cathode materials, by substituting oxygen, introduces highly influential M-F bonds due to fluorine's exceptional electronegativity (Pauling scale ~3.98) [8,37]. These bonds effectively lower the TM d-orbital energy, thereby increasing the cell's operating voltage. The extent of fluorine substitution dictates its specific benefits: trace amounts can enhance electronic conductivity, whereas substantial incorporation primarily elevates the voltage plateau and energy density. Furthermore, replacing divalent O^{2-} with monovalent F^- necessitates charge compensation, often resulting in a lower initial TM oxidation state. This expands the TM-centered redox capacity and reduces reliance on problematic oxygen redox processes, consequently improving cycling stability.

When fluorine is combined with other polyanionic groups, such as phosphates or sulfates, their individual inductive effects can synergize, leading to a further significant increase in TM redox potentials, as

exemplified by materials like $KVPO_4F$ and $Na_3V_2(PO_4)_2F_3$. This "cumulative inductive effect" underscores a broader "anion engineering" strategy, where carefully selected combinations of electronegative species are employed to precisely tailor electrochemical properties [38]. Fluorine's role is thus multifaceted, extending beyond direct voltage enhancement to influencing electronic conductivity, accessible TM valence states, and cycling stability, though its optimal incorporation strategy remains highly dependent on the specific parent material and targeted performance metrics.

2.2. Introduction of K-Polyanionic compounds as cathodes for KIBs

The successful development of polyanionic cathode materials for LIBs and NIBs, particularly Li/Na-based sulfates and phosphates, has inspired substantial research efforts toward designing high-voltage cathode materials for KIBs [39,40]. Building upon this foundation, recent breakthroughs in K-based fluorosulfate systems have emerged. Notably, the electrochemical derivation of $FeSO_4F$ from $KFeSO_4F$ represents a significant advancement, demonstrating reversible intercalation of 0.8 K^+ ions per formula unit within an elevated potential window of 2–5 V vs. K^+/K when employing 1 M $KClO_4$ in propylene carbonate electrolyte [41]. This achievement marks the first reported fluorosulfate cathode for KIBs.

Parallel developments in phosphate-based systems have revealed both promise and challenges. While Mathew et al. pioneered amorphous $FePO_4$ cathodes achieving a remarkable capacity of 156 mAh g^{-1} at 2.5 V (3.5–1.5 V vs. K^+/K), the suboptimal working potential of these low-crystalline heterosite structures highlights the need for improved redox engineering [42]. These findings nevertheless underscore the potential of potassium transition metal phosphates (KTM PO_4, TM = Fe, Mn) as viable cathode candidates. Despite established synthesis protocols and structural understanding for these materials, their electrochemical mechanisms remain ambiguous, with recent studies by Hosaka et al. suggesting pseudocapacitive-like behavior rather than conventional intercalation processes [16].

The exploration of vanadium-based polyanionic compounds has yielded more systematic progress. Han et al. developed $K_3V_2(PO_4)_3$/C composites delivering 55 mAh g^{-1} at ~3.5 V, while Lin et al. achieved enhanced performance through fluorine substitution in $K_3V_2(PO_4)_2F_3$ (capacity >100 mAh g^{-1} at ~3.7 V) via electrochemical ion exchange from its Na analogue. Subsequent material screening efforts identified KVP_2O_7 pyrophosphate as a particularly promising candidate, exhibiting 60 % K^+ reversibility and an exceptional average discharge voltage of 4.2 V at 0.25 C, albeit with moderate capacity (60 mAh g^{-1}) [43]. Chihara's work further expanded this family through metastable fluorophosphates and oxyphosphates operating in the 4 V-class regime (92 and 84 mAh g^{-1} respectively), establishing new benchmarks for high-voltage KIB cathodes [44].

Interestingly, titanium-based polyanionics are traditionally confined to anode applications due to their low redox potentials, which have recently demonstrated unexpected cathode potential through synergistic polyhedral engineering. The combination of strong polyanionic (PO_4^{3-}) and fluoride inductive effects enabled Ti^{4+}/Ti^{3+} redox activity at 3.6–3.7 V vs. K^+/K, illustrating the critical role of electronegative substituents in modulating transition metal redox potentials. This design principle was further validated in rhombohedral $K_xFe_2(SO_4)_3$ systems, achieving 100 mAh g^{-1} at 3.3 V through optimized sulfate frameworks [45].

Current research landscape analysis reveals concentrated efforts on Fe-, V-, and Ti-containing phosphate/pyrophosphate/sulfate systems, with demonstrated capacities typically below 160 mAh g^{-1}. While these proof-of-concept studies establish fundamental structure-property relationships, significant challenges remain in balancing energy density, rate capability, and cycling stability. Systematic exploration of unexplored polyanionic chemistries, coupled with advanced electrolyte engineering and nanostructuring approaches, will be essential to develop practical high-performance KIB cathodes. Particular emphasis should be placed on expanding the transition metal palette beyond current limitations while maintaining the inherent voltage advantages of polyanionic frameworks.

2.3. Classification of K-Polyanionic cathode materials

2.3.1. Phosphate

NASICON-type polyanionic compounds, originating from the $Na_{1+x}Zr_2Si_xP_{3-x}O_{12}$ system renowned for its exceptional sodium-ion conductivity, have emerged as a promising framework for KIB cathodes [46]. The inherent stability of this architecture arises from the covalent $(PO_4)^{3-}$ network, which not only ensures structural integrity during cycling but also enhances working voltages through the inductive effect, outperforming conventional layered structures in both energy density and cycle life [47]. While vanadium-based NASICON materials like $Li_3V_2(PO_4)_3$ (LVP) and $Na_3V_2(PO_4)_3$ (NVP) have been extensively studied for lithium/sodium-ion systems, their potassium analogues remained underexplored until Mai's group pioneered $K_3V_2(PO_4)_3$/C composites in 2015 via an organic acid-assisted synthesis route [48]. This breakthrough triggered systematic investigations into synthesis optimization. Han et al. demonstrated that sol-gel derived $K_3V_2(PO_4)_3$/C nanoparticles (5 nm) dispersed in carbon matrices achieve 52 mAh g^{-1} capacity at 20 mA g^{-1} (2.5–4.03 V vs K^+/K), tripling the performance of solid-state synthesized bulk counterparts [43]. The enhanced kinetics, evidenced by increased diffusion coefficients and reduced charge-transfer resistance in electrochemical impedance spectroscopy (EIS), underscore the critical role of nanoscale engineering in these systems. Similarly, in-situ carbon layer-coated $K_3V_2(PO_4)_3$ particles (20–55 nm) were prepared by a facile sol-gel synthesis technique and the stretching vibrations of $(PO_4)^{3-}$ and carbon-oxygen functional groups were confirmed by FTIR spectroscopy. The electrochemical results demonstrate the excellent cycling stability of the composite electrode [49]. Additionally, Luo et al. developed carbon coated orthorhombic $K_3V_3(PO_4)_4$/C and verified its low temperature performance. The results show that the carbon coating can induce the formation of a stable CF_3-rich protective layer at the interface between the cathode and the electrolyte, which significantly reduces the charge transfer resistance of the electrode, prevents the electrode from cracking, and ensures the redox stability of the $K_3V_3(PO_4)_4$/C during the cycling process of V^{3+}/V^{4+}[50].

Material innovation has progressed through three principal strategies: conductive network design, cationic substitution, and morphological control. Zhang's development of triple carbon-coated $K_3V_2(PO_4)_3$ (amorphous carbon/CNT/rGO) exemplifies the first approach, achieving remarkable cycling stability with 0.06 % capacity decay per cycle over 500 cycles at 5 C through synergistic electron transport and strain accommodation [51]. In parallel, Rb^+ doping at potassium sites ($K_{2.95}Rb_{0.05}V_2(PO_4)_3$/C) expanded ionic diffusion channels, boosting initial capacity by 35 % (55.7 vs 41.1 mAh g^{-1}) and cycle retention from 78.1 % to 94.4 % via enlarged lattice parameters [52]. Morphological optimization reached new heights with Jerome et al.'s spray-dried monoclinic $K_3V(PO_4)_2$/C composites (P21/c space group), where in-situ carbon integration during particle formation (2 μm spheres) coupled with post-synthesis grinding yielded 101 mAh g^{-1} at C/40 rate a 90 % utilization of the theoretical 150 mAh g^{-1} capacity enabled by the higher K/V ratio in this variant [53].

The versatility of NASICON frameworks is further demonstrated in symmetric full-cell configurations. Zhang's team utilized KVP/C as both anode (0.01–2.5 V) and cathode (2.0–4.0 V), leveraging vanadium's multivalent redox activity ($V^{3+}\leftrightarrow V^{4+}\leftrightarrow V^{5+}$) to achieve 130 mAh g^{-1} and 85 mAh g^{-1} capacity retention in respective electrodes over 150 cycles [54]. This bifunctionality extends to titanium-based systems, where Voronina et al. engineered rhombohedral $KTi_2(PO_4)_3$@C (R-3c) through precipitation synthesis and summarized the mechanistic properties of the NASICON-type $ATi_2(PO_4)_3$ structure (A = Li, Na, or K) (Fig. 4).

Carbon coating dramatically enhanced conductivity from 5×10^{-6} to 7×10^{-3} S cm^{-1}, enabling reversible Ti^{4+}/Ti^{3+} redox across 1–4 V with stable K^+ (de)intercalation (2 mol per formula unit) [55]. Furthermore, Dong et al. constructed porous self-supported composite electrodes of N-doped carbon nanofibers wrapped with $KTi_2(PO_4)_3$ nanoparticles by electrostatic spinning. The porous N-doped interconnected carbon fibers provided a short transport path and a bulk buffer layer for potassium ions, exhibiting excellent rate performance (99.3 mA h g^{-1} at 10 C) and superb cycling performance (no capacity decay after 300 cycles at 5 C) [56]. To overcome the cycling stability of KIB cathodes at high power density, Zhang et al. constructed a series of $K_2Ti_2(PO_4)_3$ (KTP) and $KTiOPO_4$ (KTOP) heterojunctions by selectively phosphorylating metal-organic frameworks (MOFs) through careful structural and compositional control, successfully verifying the synergistic cooperation between the electron and ion transport kinetics. Comparative analysis of density-functional theory calculations shows that the synergistic modulation can significantly promote the reaction kinetics and pseudocapacitive behavior [57].

In addition to the aforementioned K-based NASICON structure, Liu et al. prepared layered mesoporous $Mn_{0.5}Ti_2(PO_4)_3$@C microspheres by electrospray method. The introduction of carbon and the layered mesoporous structure could enhance the electrical conductivity of the composite electrode and facilitate the rapid insertion and extraction of K^+, thus exhibiting excellent cycling performance (148 mAh g^{-1} at 500 mA g^{-1} after 1000 cycles) [58]. Moreover, Dai et al. prepared $Mn_{0.5}Ti_2(PO_4)_3$/C nanofiber flexible electrodes by electrospinning, which exhibited high specific capacity and ultra-long cycling stability of >2000 cycles. First-principle calculations demonstrated that $Mn_{0.5}Ti_2(PO_4)_3$ exhibited a lower energy gap than $KTi_2(PO_4)_3$, making it more suitable for potassium ion storage [59]. Such advancements highlight the NASICON architecture's adaptability across multiple redox-active metals, positioning it as a cornerstone for next-generation KIB cathodes through continued optimization of electronic/ionic transport networks and redox couple utilization.

2.3.2. *Oxyphosphate*

Oxyphosphate materials occupy a unique position in cathode development for KIBs, bridging the electrochemical advantages of oxides and phosphates through optimized mass-to-charge ratios that enable higher theoretical capacities compared to conventional ortho- or condensed phosphates. Among these candidates, $KVOPO_4$ has emerged as the most promising oxyphosphate cathode, crystallizing in an orthorhombic $Pna2_1$ structure characterized by corner-sharing VO_6 octahedra and PO_4 tetrahedra along the [011] and [011] directions, with potassium ions occupying two equivalent crystallographic sites. Initial breakthroughs by the Komaba group demonstrated the feasibility of $KTiOPO_4$-type $KVOPO_4$ cathodes through low-temperature solid-state synthesis, overcoming traditional limitations of high-temperature processing while achieving micron-scale particle control (2–10 μm) [44]. Electrochemical evaluation in 1 M KPF_6 EC:DEC (1:1 v/v) electrolyte revealed a discharge capacity of 84 mAh g^{-1} within 2.0–4.8 V vs K^+/K, coupled with exceptional rate retention (93.9 % capacity at 5 C), primarily attributed to vanadium redox activity above 4.0 V. The uncontrollable nature of solid-state synthesis produces primary impurity defects, which can lead to high-voltage performance failures and severe cycling degradation. Therefore, Li et al. prepared pure-phase $KVOPO_4$ materials by combining the carbothermal reduction method and the strategy of voltage regulation to stabilize the electrode/electrolyte interface. The obtained $KVOPO_4$ has a stable three-dimensional crystal framework and abundant active sites, which is conducive to the realization of efficient and continuous K^+ diffusion (Fig. 5) [60]. Complementing these experimental findings, Lian et al. conducted density functional theory (DFT) calculations that validated the two-phase transition mechanism during potassium extraction [61]. The study identified sequential structural evolution in $K_{1-x}VOPO_4$ ($0 \leq x \leq 1.0$) through orthorhombic Pna21 intermediates, with distinct phase boundaries at $0 \leq x \leq 0.5$ and $0.0625 < x \leq 0.75$, consistent with observed electrochemical signatures.

In addition to $KVOPO_4$, $KTiOPO_4$ has been widely studied as a promising oxyphosphate. Qi et al. synthesized $KTiOPO_4$ nanoparticles with favorable crystallinity in the absence of carbon coatings and high temperature treatment. Benefiting from the stable structural framework and highly reversible K^+ (de)insertion process, the prepared $KTiOPO_4$ electrodes exhibited impressive electrochemical performance in KIB, including high specific capacity, excellent rate capability and cycling stability [62]. Furthermore, Kumar et al. synthesized $KTiOPO_4$-rGO composite electrodes and investigated the potassium storage properties of the composite electrodes using fluorosulfonamide electrolyte and sodium alginate binder. Operando and ex-situ XRD measurements confirmed the multiple structural changes of $KTiOPO_4$-rGO during the electrochemical process as well as the highly reversible nature of the phase evolution [63]. To investigate the performance of $KTiOPO_4$ as a KIB cathode material, Huang et al. performed first-principles calculations of the stability and electronic properties of the deassassified structure as well as potassium de-embedding and diffusion mechanism probes. The anionic oxygen oxidation–reduction in KTP provides a K/K^+ voltage ratio of >4 V and a low ion diffusion resistance (0.29 eV) by the PBE+U method, suggesting that KTP has favorable rate performance as a

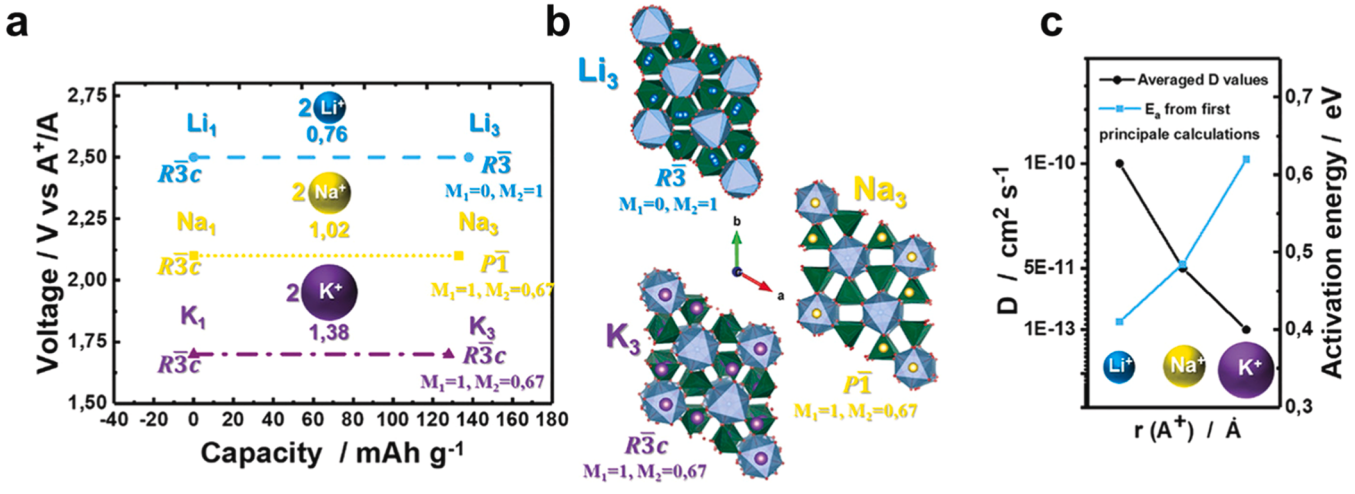

Fig. 4. Comparative representation of properties in $ATi_2(PO_4)_3 \leftrightarrow A_3Ti_2(PO_4)_3$ system: (a) voltage versus theoretical capacity; (b) crystal structures of $A_3Ti_2(PO_4)_3$; (c) diffusion coefficient values. Reproduced with permission [55] Copyright 2020 WILEY-VCH Verlag GmbH & Co. KGaA, Weinheim. All rights reserved.

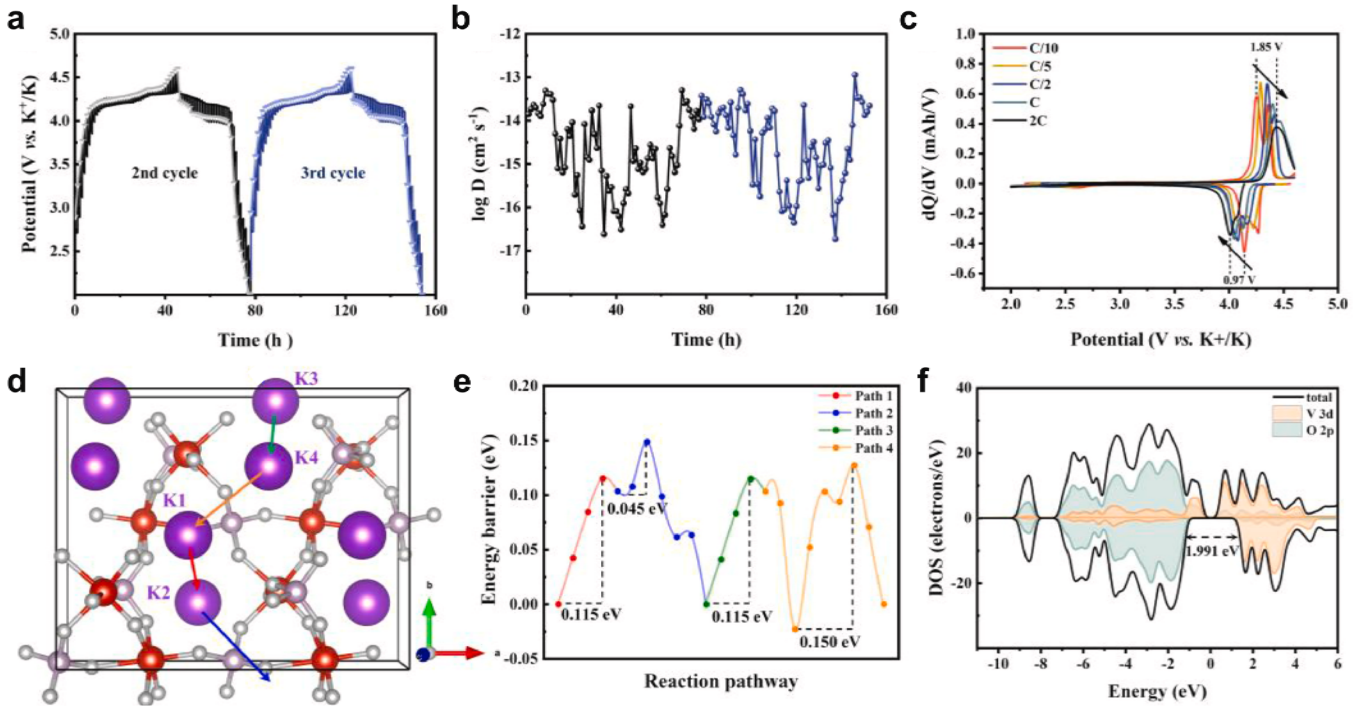

Fig. 5. Charge/discharge profiles of $KVOPO_4$ during the 2nd and 3rd cycles in GITT measurements. (b) Corresponding K^+ diffusion coefficient derived from (a). (c) dQ/dV curves recorded at various scan rates during the 5th cycle. (d) Diffusion pathways of K^+ in the $KVOPO_4$ structure. (e) Corresponding K^+ migration energy barriers calculated using PBE+*U*. (f) Total density of states of $KVOPO_4$ along with the partial density of states for O 2p and V 3d orbitals. Reproduced with permission [60] Copyright 2023 Elsevier B.V. All rights reserved.

KIB cathode [64]. This theoretical framework provides critical insights into the material's solid-solution behavior and voltage profile characteristics, establishing a foundation for future optimization of potassium storage kinetics in oxyphosphate systems.

2.3.3. *Fluorophosphate*

Fluorophosphate-based cathodes, particularly $KMPO_4F$ ($M = V$, Fe) and $K_3V_2(PO_4)_2F_3$, have emerged as promising candidates for KIBs due to their unique structural advantages and tunable electrochemical properties. The substitution of fluorine into polyanionic frameworks enhances redox potentials by modifying local atomic environments while maintaining stable three-dimensional architectures conducive to K^+ diffusion. $KVPO_4F$, a prototypical fluorophosphate with a $KTiOPO_4$-type structure ($Pna2_1$ space group), features corner-sharing VO_4F_2 octahedra interconnected by PO_4 tetrahedra, forming rigid channels for ionic transport. Pioneered by Fedotov et al. through freeze-drying-assisted synthesis, $KVPO_4F$/C composites demonstrated reversible Li/K ion exchange in lithium systems before being adapted for KIBs [65]. Subsequent optimizations by Chihara et al. via solvothermal routes yielded micron-scale particles (2–15 μm) delivering 92 mAh g^{-1} at 4.02 V average potential in 0.7 M KPF_6 EC:DEC electrolyte, leveraging sequential $V^{3+}/V^{4+}/V^{5+}$ redox activity [44]. First-principles calculations by Kim et al. revealed a 6.54 % lattice contraction during full K^+ extraction, attributed to V^{4+} oxidation and K^+ removal, while oxygenation studies showed disordered anion arrangements suppress K^+/vacancy ordering, enabling smoother voltage profiles [66]. Despite achieving 454 Wh kg^{-1} energy density, $KVPO_4F$ suffers from limited cyclability due to intrinsic low conductivity (1.84×10^{-5} S m^{-1}) and interfacial instability. Liu et al. addressed these challenges through a 3D amorphous carbon network ($KVPO_4F$@3DC), achieving 85.4 % capacity retention over 550 cycles at 500 mA g^{-1} via enhanced electron transport and interfacial stabilization (Fig. 6**a and b**) [67]. In addition, Xie et al. fabricated a dense, hierarchical microsphere structure of $KVPO_4F$ with a pomegranate-like carbon coating. The nano-sized primary particles within the $KVPO_4F$ microspheres significantly enhance the diffusion kinetics of K^+ compared to bulk materials, thereby improving the rate performance [68]. In addition to the single carbon-coating strategy, Liao et al. prepared carbon-coated single-crystalline $KVPO_4F$ nanoplates based on a vanadium–oxalate–phosphite/phosphate framework and fluorinated polymer. The V-F-C bond formed at the interface of the $KVPO_4F$/C nanoplates effectively reduces the loss of fluorine (F) during the electrochemical process, while enhancing the transport kinetics and electronic conductivity of the electrode [69].

The modification of $KVPO_4F$ has become a hot research direction for KIB cathodes in recent years. Heng et al. developed a high-energy and low-strain $KVPO_4F$ composite cathode assisted by a multifunctional $K_2C_4O_4$ electrode stabilizer. The $K_2C_4O_4$ additive enables in-situ potassium compensation and carbon deposition through a self-sacrificing reaction, which synergistically enhances the electrochemical performance. In-situ and ex-situ characterizations reveal that the $KVPO_4F$ electrode exhibits minimal volume strain (approximately 5 %) and a thin, uniform cathode–electrolyte interphase, contributing to its improved stability [70]. The sluggish kinetics and pronounced volume change of $KVPO_4F$ are the primary barriers leading to irreversible structural damage, elevated internal resistance, and inferior cycling stability. Zhao et al. addressed these challenges by employing a Cs^+ doping strategy, which effectively reduces the energy barriers associated with ion diffusion and volume change during potassiation and depotassiation processes. Consequently, the resulting $K_{0.95}Cs_{0.05}VPO_4F$ cathode exhibits superior discharge capacity and enhanced cycling life [71]. The unique electron transfer pattern in the covalent bond structure of $KVPO_4F$ leads to poor bulk kinetics. To address this issue, Zhu et al. introduced a large-sized weak-field ligand, Cl^-, to adjust the coordination environment of the V octahedron, synthesizing $KVPO_4F_{0.9}Cl_{0.1}$. The larger Cl^- expanded the lattice structure, stimulating the hybridization between the V 3d orbitals and the 2p/3p orbitals of the ligands, thereby reducing the crystal field splitting energy and promoted rapid K^+ ion diffusion within the bulk material [72].

Parallel advancements in titanium-based systems yielded $KTiPO_4F$ isostructural to $KVPO_4F$ ($Pna2_1$), synthesized hydrothermally under

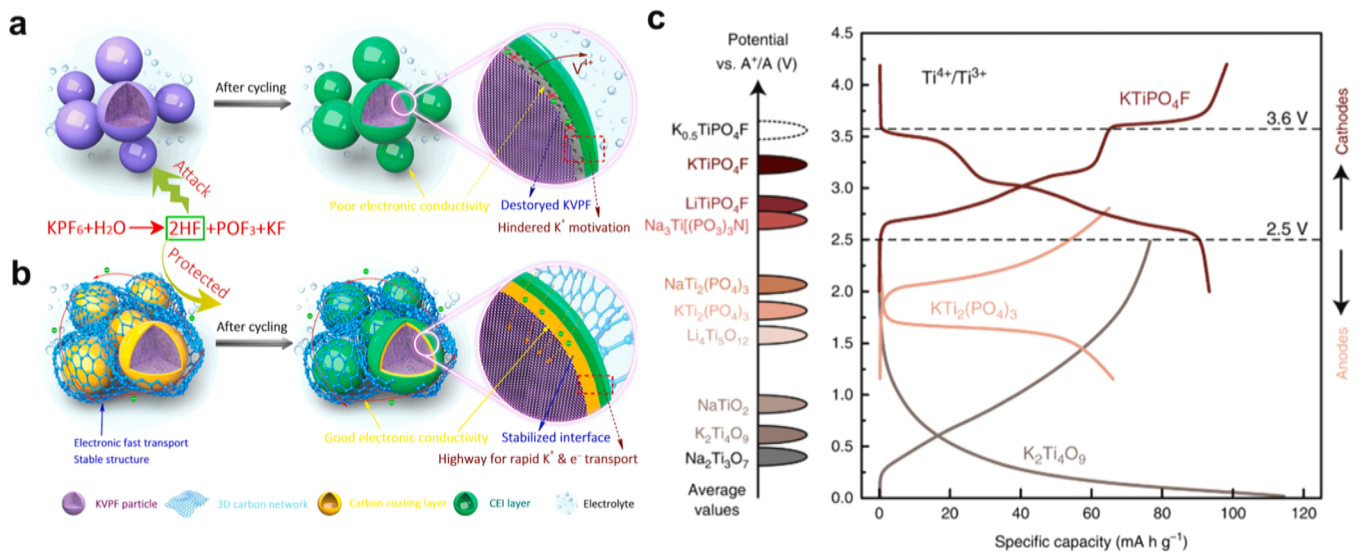

Fig. 6. Schematic diagram of the interface change during repeated charge-discharge process at elevated temperature. (a) Bare KVPF; (b) KVPF@3DC composite. Reproduced with permission [67]. Copyright 2020, Published by Elsevier B.V. and Science China Press. All rights reserved. (c) Comparison of the average operating potentials of Ti-based electrode materials and charge/discharge curves for several representatives. Dashed line at 2.5 V shows a tentative border between cathode (above) and anode (below) materials. Dashed line at 3.6 V designates the average potential of the $K_{0.5}TiPO_4F/TiPO_4F$ transition. Reproduced with permission [65]. Copyright 2020, The Author(s).

reducing conditions to stabilize Ti^{3+}. This material exhibits Ti^{4+}/Ti^{3+} redox activity at 3.6–3.7 V vs K^+/K, delivering 94 mAh g^{-1} at C/20 with reversible phase transitions observed via operando XRD during charge/discharge (Fig. 6**c**) [65]. Ramezankhani et al. synthesized $KTiPO_4F$ with a robust framework structure via a hydrothermal method. The resulting electrode operates through a solid-solution-like de/insertion mechanism, exhibiting an average potential of only 0.8 V versus K/K^+ and a cell volume change of merely 8.5 % [73]. Meanwhile, $K_3V_2(PO_4)_2F_3$

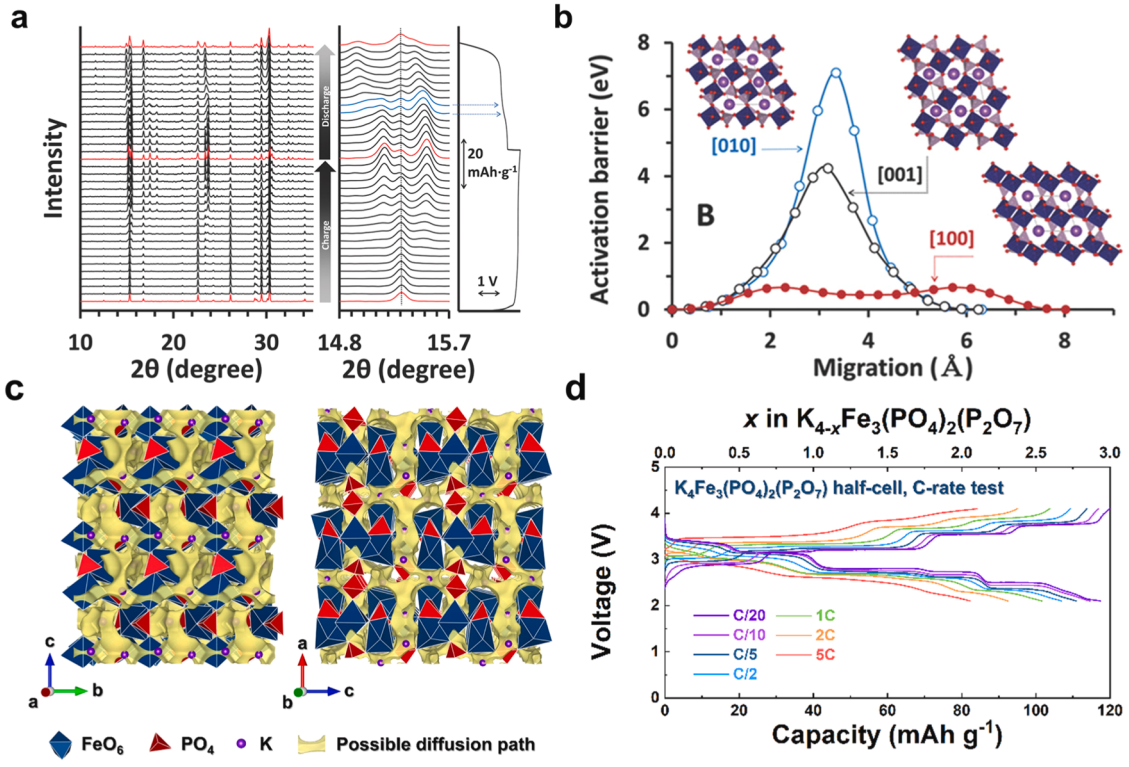

Fig. 7. (a) In situ XRD of KVP_2O_7 during a full C/D cycle (0.25 C, 20 °C). Magnified view clearly shows the (110) reflections of monoclinic P21/c (denoted by a dotted line) in all XRD patterns. The evolution of the triclinic (010) and (100) reflections of P1 with C/D (2θ 15.15° and 15.51°) are also evident. Note also that the sudden shift in the (010) and (100) peak positions to a small 2θ occurs after a sloping potential region (denoted by arrows). (b) Activation energy barriers for $K_{1-x}VP_2O_7$ (x~0.6), with insets exhibiting the projected views along the specified direction. Reproduced with permission [74]. Copyright 2020, Elsevier B.V. All rights reserved. (c) BVS energy map of $K_4Fe_3(PO_4)_2(P_2O_7)$ with all possible K-ion sites in the crystal structure. (d) The charge-discharge profiles of $K_4Fe_3(PO_4)_2(P_2O_7)$ in the voltage range of 2.1–4.1 V at various current densities [75]. Copyright 2020, Elsevier B.V. All rights reserved.

derived from $Na_3V_2(PO_4)_2F_3$ via electrochemical ion exchange (Amam → $Cmc2_1$ space group transition) demonstrates exceptional rate capability (83 mAh g^{-1} at 100 mA g^{-1}) owing to its open framework of VO_4F_2 and PO_4 polyhedra [28]. While these fluorophosphates exhibit high-voltage operation (>4 V), further performance enhancements necessitate nanoscale engineering and conductive coatings strategies proven effective in lithium systems to mitigate kinetic limitations and optimize K^+ diffusion pathways across this emerging class of polyanionic cathodes.

2.3.4. Pyrophosphate

Pyrophosphate-based cathodes, leveraging the inherent stability of $P_2O_7^{4-}$ anions, have transitioned from established lithium/sodium-ion systems to emerging KIB applications due to their superior thermal stability, cycling endurance, and rate capability. Initial KIB investigations focused on KVP_2O_7, first reported by Park et al. through solid-state synthesis of seven candidate pyrophosphates [74]. Among these, KVP_2O_7 demonstrated reversible 0.6 K^+ extraction (48 mAh g^{-1}) at 4.14–4.48 V via V^{3+}/V^{4+} redox, accompanied by a monoclinic (P21/c) to triclinic (P1) phase transition during deintercalation (Fig. 7**a**). Structural analysis revealed metastable $K_{1-x}VP_2O_7$ (x∼0.6) phases capable of reverting to the original framework upon thermal or electrochemical treatment, highlighting the structural resilience of pyrophosphate frameworks (Fig. 7**b**).

2.3.5. Mixed phosphate

Building on this foundation, mixed polyanion systems incorporating dual anion groups (e.g., PO_4^{3-}-$P_2O_7^{4-}$) have emerged as high-performance alternatives. Kim's group pioneered $K_4Fe_3(PO_4)_2(P_2O_7)$ via electrochemical ion exchange, overcoming synthesis challenges associated with direct methods [76]. The orthorhombic ($Pn2_1a$) structure features $[Fe_3P_2O_{13}]_\infty$ layers with interconnected FeO_6 octahedra and P_2O_7 units, creating 3D K^+ diffusion channels that enable 118 mAh g^{-1} at C/20 (70 % capacity retention at 5 C) with a 3.21 V average potential (Fig. 7**c and d**). Parallel work by Barpanda et al. adapted NASICON-type $Na_4Fe_3(PO_4)_2P_2O_7$ for KIBs through desodiation, achieving 120 mAh g^{-1} at 3 V with minimal volume expansion (5.6 %) during $NaFe_3(PO_4)_2P_2O_7$ formation [76]. Full-cell configurations pairing this cathode with graphite anodes demonstrated stable cycling, underscoring practical viability. Expanding the transition metal palette, Mn-substituted $K_4Mn_2Fe_2(P_2O_7)$ synthesized via analogous ion-exchange methods delivered 110 mAh g^{-1} at 3.5 V through sequential Fe^{2+}/Fe^{3+} (2.0 V) and Mn^{2+}/Mn^{3+} (3.1–4.3 V) redox activity [77]. The material's orthorhombic framework ($Pn2_1a$) maintained 83 % capacity over 300 cycles at C/3, attributed to rigid $[Mn,Fe]O_6$-PO_4 connectivity minimizing structural strain during K^+ (de)intercalation. These advancements establish mixed pyrophosphate-phosphates as versatile platforms for high-voltage KIB cathodes, though challenges persist in optimizing electronic conductivity and scaling synthesis protocols for industrial adoption.

2.3.6. Sulfate and fluorosulfate

Sulfate and fluorosulfate polyanions have emerged as high-voltage cathode candidates for KIBs, leveraging their exceptional electronegativity to elevate redox potentials. Among polyanionic groups, sulfate $(SO_4)^{2-}$ exhibits the highest electronegativity [$(SiO_4)^{4-}$ < $(CO_3)^{2-}$ < $(PO_4)^{3-}$ < F^- < $(P_2O_7)^{4-}$ < $(SO_4)^{2-}$], a property driven by the strong inductive effect of covalent S–O bonds that enhances operating voltages. Early exploration of fluorosulfate by Tarascon et al. identified orthorhombic $KFeSO_4F$ (KTP-type structure) as a pioneering cathode material synthesized via solid-state methods [42]. This Fe-based fluorosulfate demonstrated reversible extraction/insertion of 0.8 K^+ per formula unit within a 4.8 V window using 1 M $KClO_4$/PC electrolyte, though mechanistic studies on its charge storage behavior remain incomplete. Parallel developments in sulfate systems yielded yavapaiite-type $K_xFe(SO_4)_2$ (C2/m space group), synthesized through low-temperature calcination of aqueous precursors [78]. Its quasi-layered framework, comprising FeO_6 octahedra and SO_4 tetrahedra along the ab-plane, enables reversible Fe^{2+}/Fe^{3+} redox at 3.3 V average potential, delivering 94 mAh g^{-1} at C/20 with minimal volume change (1.83 %) during cycling. As shown in Fig. 8, operando XRD confirmed single-phase K^+ (de)intercalation in $K_{1+x}Fe(SO_4)_2$, underpinning its exceptional cyclability (80 % capacity retention after 300 cycles at 2 C). Kumar et al. modulated the crystallinity and ionic/electronic conductivity of $KFeSO_4F$ by doping magnesium ions (Mg^{2+}) at the iron sites. Studies combining UV–vis absorption spectroscopy with X-ray diffraction and absorption spectroscopy revealed that Mg-doped $KFeSO_4F$ powder samples exhibited a narrower bandgap and a multiphase redox mechanism involving Fe^{3+}/Fe^{2+} compared to the undoped material [79]. Liao et al. first reported the fabrication of $KFeSO_4F$ microspheres interwoven with carbon nanotubes (CNTs) in diethylene glycol (DEG). The strong binding affinity of the ether groups in DEG retards the nucleation and growth of $KFeSO_4F$, enabling the in-situ interweaving of CNTs within the $KFeSO_4F$ crystals. The extensive exposure of the (100) crystal plane and the uniform penetration of CNTs within the microspheres significantly enhance the electronic conductivity and electrochemical performance of $KFeSO_4F$ [80]. The superior performance of sulfate-based cathodes over conventional Fe-layered oxides highlights the critical role of SO_4 polyanions in stabilizing high-voltage redox couples while accommodating large K^+ ions. These advances position sulfate/fluorosulfate systems as promising high-energy-density candidates, though challenges persist in optimizing ionic conductivity and elucidating full reaction pathways for practical implementation.

A summary of representative polyanion-type electrode materials concentrating on the structure, voltage window, average voltage, specific capacity, cycle property, and rate performance is provided in Table 2 and the spider map is schematically illustrated in Fig. 9.

From a capacity perspective, although performance varies depending on the polyanion compound structures, most potassium polyanion compounds cathode exhibits initial reversible capacities in the range of 80–120 mAh g^{-1} due to their relatively large molar mass and the limited reversible intercalation/deintercalation of K^+ ions [16]. In terms of average voltages, oxyphosphate primarily derive their capacity from the V^{4+}/V^{5+} redox couple, thereby achieving higher operating voltages compared to phosphate structures based on the V^{3+}/V^{4+} couple [87]. Furthermore, F-based fluorophosphate and fluorosulfate exhibit further enhanced average operating voltages, approaching 4.0 V, as a result of the inductive effect of F^- [88]. All polyanionic cathodes generally possess robust 3D frameworks and strong covalent bonding, which contribute to their excellent cycling stability [89]. Among these, $KFeSO_4$ stands out with a remarkable cycling retention of 93.9 % over 2000 cycles [89]. In terms of rate capability, the tetragonal $KVOPO_4$ cathode delivers a high discharge capacity of 83.4 mAh g^{-1} even at a high current density of 2400 mA g^{-1}. Compared to phosphate-based compounds, sulfates and fluorosulfates exhibit lower economic values due to their sensitivity to moisture and the challenges involved in both synthesis and post-synthesis handling [90]. Moreover, structures such as phosphate, pyrophosphate, oxyphosphate, and fluorophosphate typically rely on vanadium as the transition metal [91]. Given that vanadium is both expensive and toxic, these materials demonstrate lower economic feasibility compared to mixed phosphate systems that utilize iron as the transition metal.

Among various polyanion-type materials for KIBs, no single cathode material has yet demonstrated simultaneously high capacity, excellent cycling stability, outstanding rate capability, and elevated average operating voltage (Fig. 10). To improve the trade-offs among various electrochemical parameters, it is crucial to achieve performance uniformity through the optimization of synthesis methods and conditions. Furthermore, the electrochemical properties can be further enhanced through strategies such as carbon coating and metal doping.

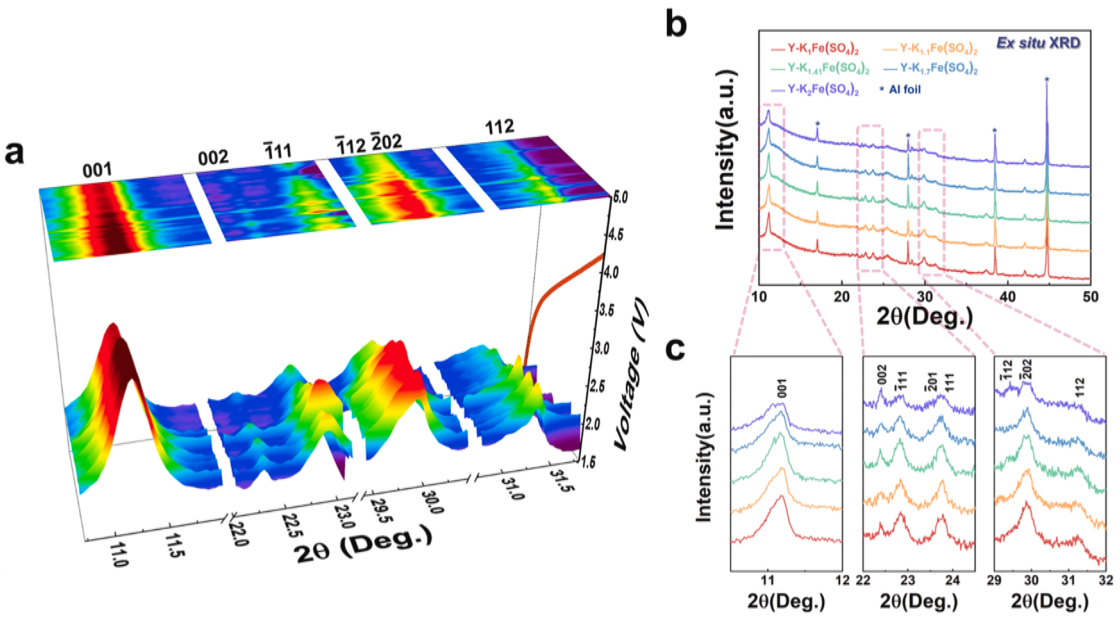

Fig. 8. (a) Operando XRD pattern of Y-$K_xFe(SO_4)_2$ ($1 \leq x \leq 2$). (b), (c) Ex-situ XRD patterns of Y-$K_xFe(SO_4)_2$ ($1 \leq x \leq 2$). Reproduced with permission [78]. Copyright 2019, Elsevier Ltd. All rights reserved.

Table 2
Comparison between different types of polyanion compounds cathodes for KIBs.

Polyanion compounds		Structure	Potential/V (vs K/K^+)	Specific capacity	Capacity retention	Rate capability
Phoshphate	$K_3V_2(PO_4)_3$/C [11]	Orthorhombic	~3.5V	87mAh g^{-1} (20 mA g^{-1})	51.5 % (100cyc, 200 mA g^{-1})	37mAh g^{-1} (400 mA g^{-1})
	$K_3V_2(PO_4)_3$/C [44]	Monoclinic	~3.8V	42mAh g^{-1} (20 mA g^{-1})	87 % (30cyc, 50 mA g^{-1})	15mAh g^{-1} (200 mA g^{-1})
	$KFePO_4$/C [49]	Monoclinic	~ 2.9V	100mAh g^{-1} (10 mA g^{-1})	90 % (50cyc, 10 mA g^{-1})	–
	$KTi_2(PO4)_3$ /C [55]	Orthohombic	~1.7V	126mAhg^{-1} (20 mA g^{-1})	89 % (500cyc, 200 mA g^{-1})	75 mA g^{-1} (128 mA g^{-1})
Oxyphosphate	$KVOPO_4$ [76]	Tetragonal	~3.65V	115mAh g^{-1} (24 mA g^{-1})	~86.8 % (100cyc, 60 mA g^{-1})	83.4 mA g^{-1} (2400 mA g^{-1})
	$KVOPO_4$ [60]	Orthohombic	~4.2V	73mAh g^{-1} (56 mA g^{-1})	86 % (1000cyc, 28 mA g^{-1})	~55mAh g^{-1} (226 mA g^{-1})
Fluorophosphate	$KVPO_4F$ [81]	Orthorhombic	~4.3V	95mAh g^{-1} (20 mA g^{-1})	92 % (120cyc, 20 mA g^{-1})	–
	$K_3V_2O_2(PO_4)_2F$ [82]	Orthorhombic	~3.9V	105mAh g^{-1} (100 mA g^{-1})	93.5 % 200 cyc, 100 mA g^{-1})	40mAh g^{-1} (5000 mA g^{-1})
Pyrophosphate	$K_2(VO)_3(P_2O_7)_2$ [83]	Orthorhombic	~3.9V	84mAh g^{-1} (10 mA g^{-1})	92 % (50cyc, 10 mA g^{-1})	62mAh g^{-1} (85 mA g^{-1})
	$K_2VOP_2O_7$ [84]	Tetragonal	3.6 V	89mAh g^{-1} (20 mA g^{-1})	65 % (50cyc, 50 mA g^{-1})	35mAh g^{-1} (100 mA g^{-1})
Sulfate	Y-$KFe(SO_4)_2$ [78]	Monoclinic	~3.5V	110mAh g^{-1} (4.9 mA g^{-1})	80 % (300cyc, 190 mA g^{-1})	65mAh g^{-1} (470 mA g^{-1})
	$K_2Fe_3(SO_4)_3$ $(OH)_2(H_2O)_2$ [85]	Orthorhombic	~2.75V	120mAh g^{-1} (20 mA g^{-1})	80 % (100cyc, 100 mA g^{-1})	45mAh g^{-1} (2000 mA g^{-1})
	$K_4Fe_3(C_2O_4)_3(SO_4)_2$ [86]	Monoclinic	2.9V	80mAh g^{-1} (100 mA g^{-1})	80 % (100cyc, 100 mA g^{-1})	54mAh g^{-1} (500 mA g^{-1})
Fluorosulfate	$KFeSO_4F$ [80]	Orthorhombic	3.73V	110.9mAh g^{-1} (25.6 mA g^{-1})	93.9 % (2000cyc, 384 mA g^{-1})	69.6mAh g^{-1} (2560 mA g^{-1})
Mixed phosphate	$K_4Fe_3(PO_4)_2(P_2O_7)$ [76]	Orthorhombic	~3.21V	118mAh g^{-1} (6 mA g^{-1})	82.0 % (500cyc, 600 mA g^{-1})	82mAh g^{-1} (600 mA g^{-1})
	$K_4Mn_2Fe_1$ $(PO_4)_2(P_2O_7)$ [77]	Orthorhombic	3.5V	110mAh g^{-1} (5.8 mA g^{-1})	83 % (300cyc, 39 mA g^{-1})	85mAh g^{-1} (585 mA g^{-1})

3. Viewpoints of K-polyanionic compounds

3.1. Selection of material synthesis

The synthesis of potassium-based polyanionic cathode materials presents unique challenges due to the interplay between bulky K^+ ions (1.38 Å ionic radius) and rigid polyanionic frameworks, which often lead to reduced theoretical capacities and complex crystallization dynamics. Conventional solid-state reactions (SSR), while cost-effective and scalable for mass production, frequently yield materials with poor crystallinity, non-uniform particle distribution, and high energy consumption limitations exacerbated in KIB systems. Despite these

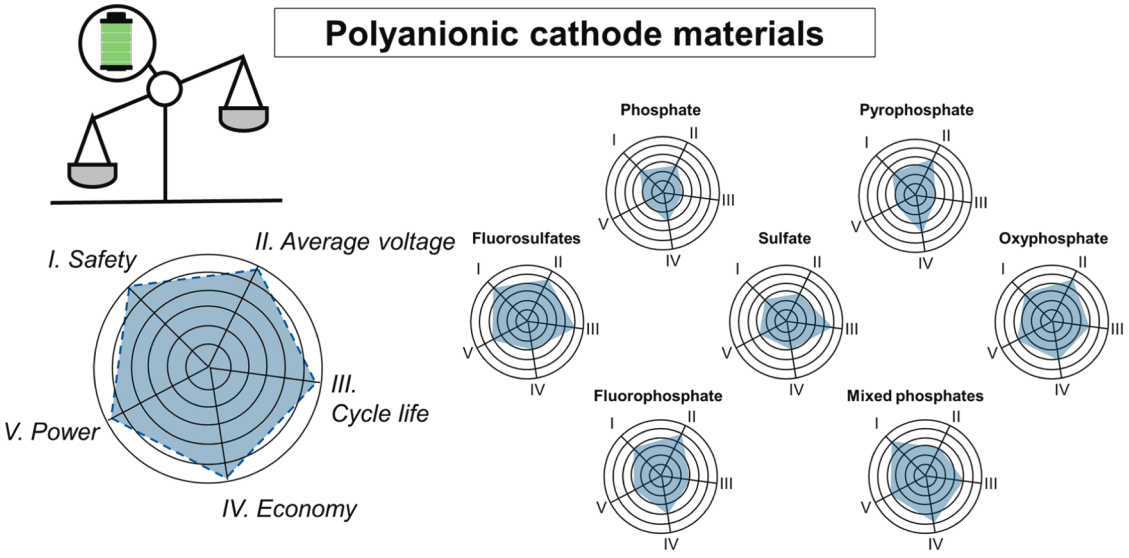

Fig. 9. Schematic illustration of polyanionic cathode material using spider map. (I: Safety, II: Average voltage, III: Cycle life, IV: Economy, V: Power).

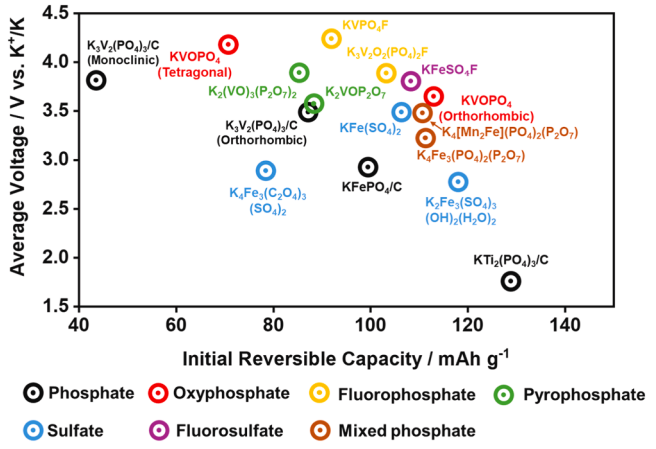

Fig. 10. Summarization of the parameters including initial reversible capacity and average voltage of polyanion compound cathodes for KIBs.

drawbacks, SSR remains widely employed for synthesizing compounds like $KFePO_4$ and $KVPO_4F$, typically requiring high-temperature calcination (700–850 °C) under inert atmospheres. Hydrothermal methods offer a complementary approach, enabling controlled morphology and nanosized particles (e.g., $KTiPO_4F$, $K_2Fe_3(SO_4)_3(OH)_2(H_2O)_2$) at moderate temperatures (130–250 °C) through aqueous-phase reactions under autogenous pressure. This technique proves particularly advantageous for enhancing the cycling stability and rate capability of low-conductivity polyanions, though scalability remains constrained by specialized equipment requirements.

Sol-gel processing bridges the gap between particle size control and stoichiometric precision, leveraging chelating agents like citric acid to achieve in-situ carbon-coated nanocomposites. Zhang et al. demonstrated this with $K_3V_2(PO_4)_3$/C cathodes, where dual acid roles vanadium reduction and carbon source yielded porous microstructures via controlled pyrolysis [46]. Co-precipitation methods further expand the toolkit, producing nanoscale materials (e.g., $KTi_2(PO_4)_3$, ~200 nm particles) with uniform carbon coatings through solvent evaporation and low-energy calcination, albeit with compromised cycle life compared to hydrothermal analogues. For structurally elusive compounds, electrochemical ion exchange emerges as a pivotal strategy, converting Na-based precursors (e.g., $Na_3V_2(PO_4)_2F_3$) into KIB-compatible cathodes ($K_3V_2(PO_4)_2F_3$) via sequential de-sodiation and potassiation a process critical for materials unobtainable through direct synthesis.

Emerging techniques such as spray-drying offer scalable routes for fabricating multicomponent composites. For instance, Bodart et al. demonstrated the synthesis of KVP/C composites with CNT/rGO networks, achieving particles of 2.5 μm in size that feature enhanced conductive pathways [48]. Across all methods, the universal objectives remain: (1) nanostructuring to mitigate K^+ diffusion limitations, (2) carbon integration to offset inherent low conductivity (~10^{-5} S cm^{-1} for $KVPO_4F$), and (3) precise stoichiometric control to maximize redox potentials. Kim et al.'s optimized $KVPO_4F$ (4.33 V, 105 mAh g^{-1}) exemplifies how oxygen substitution avoidance in fluorophosphates preserves anion ordering, outperforming disordered variants (4.13 V, 92 mAh g^{-1}) through meticulous synthesis design [81]. These advancements underscore the necessity of method-specific optimization to balance electrochemical performance with practical manufacturability in KIB cathode development.

Table 3 demonstrates the comparative characteristics of these methods based on cost, uniformity, purity, energy consumption, production scalability, and environmental impact. While these methods can bridge the gap between scalability and material complexity, they remain in the early stages of optimization, requiring further research and process refinement for industrial viability.

3.2. Selection of suitable electrolyte

The critical role of electrolytes in KIBs extends beyond mere ion transport, profoundly influencing cycle life, rate capability, and safety through interfacial stability and oxidative resistance. While conventional carbonate-based electrolytes (e.g., KPF_6 in EC/DEC or EC/PC) dominate early KIB research, their incompatibility with high-voltage

Table 3
A summary comparison of the synthesis methods.

	Solid-state reaction	Sol-gel	Solvothermal	Spray drying
Cost	Low	High	Middle	Middle
Uniformity	Low	High	High	Middle
Purity	Low	High	High	High
Energy consumption	High	Middle	Middle	Middle
Production	High	Low	Low	High
Environment	Middle	Middle	High	High

polyanionic cathodes (>4 V vs. K^+/K) necessitates strategic reformulation. Komaba et al. demonstrated this challenge through comparative studies on $KVPO_4F$ and $KVOPO_4$ cathodes, where 1 M KPF_6 in EC/PC outperformed 0.7 M KPF_6 in EC/DEC, reducing irreversible capacity loss by 23 % at 5 V through enhanced solvent stability [44]. These findings underscore the delicate balance between salt concentration (0.5–1 M) and solvent composition, where propylene carbonate (PC) exhibits superior anodic stability (up to 4.7 V) compared to dimethyl carbonate (DMC) due to higher desolvation energy, as validated by linear sweep voltammetry.

Interfacial dynamics further complicate electrolyte selection. Antipov et al. revealed that K^+ charge transfer resistance in $KVPO_4F$ increases by 40 % relative to Na^+ analogues in identical carbonate systems, attributed to unstable cathode-electrolyte interphase (CEI) formation [92]. This instability is exacerbated in low-concentration electrolytes (<0.5 M KPF_6), where insufficient salt-derived passivation accelerates CEI degradation. Counterintuitively, Chen et al. found that high fluoroethylene carbonate (FEC) additive concentrations (50 vol %) in PC-based electrolytes suppress parasitic reactions at metallic anodes while maintaining $KVOPO_4$ cathode reversibility, achieving 89 % capacity retention over 200 cycles versus 67 % with standard 10 % FEC formulations [93]. Such non-linear additive effects highlight the need for electrolyte customization tailored to cathode chemistry.

Oxidative decomposition remains the primary limitation for high-voltage operation. Ceder's systematic evaluation of $KVPO_4F$ cyclability across four KPF_6-carbonate electrolytes revealed stark contrasts: EC/PC retained 63 % capacity after 200 cycles, while pure PC degraded to <10 % within 90 cycles due to unmitigated K metal reactivity [81]. XPS analysis traced capacity fade to CEI layers rich in KF, K_2CO_3, and polymeric organics byproducts of solvent oxidation confirmed by symmetric cell tests showing 300 % polarization increase in PC versus EC/PC. Parallel efforts exploring sulfolane (SL) and adiponitrile (AN) solvents, despite their high intrinsic stability (>5.5 V), failed due to poor CEI-forming propensity, emphasizing the necessity of kinetically stable surface films over thermodynamic solvent stability.

Emerging strategies focus on concentrated ether-based systems (e.g., 7 M potassium bis(fluorosulfonyl)imide (KFSI)- dimethoxyethane (DME)), which enable 4.3 V operation with reduced polarization but suffer from poor Coulombic efficiency (<92 %) and rapid capacity decay. Stevenson's work suggests this stems from ether solvent co-intercalation at high voltages, a phenomenon absent in carbonate systems but critical for polyanion stability [94]. Future electrolyte design must reconcile competing requirements: (1) high oxidative stability (>5 V), (2) effective CEI/SEI formation, and (3) compatibility with both high-voltage cathodes and K metal anodes. Current evidence positions fluorinated carbonate blends (e.g., EC/PC/FEC) as the most viable near-term solution, though advanced salt chemistries (e.g., potassium bis(trifluoromethanesulfonyl)imide (KTFSI), potassium difluoro(oxalato)borate (KDFOB)) paired with stabilizers like tris(trimethylsilyl) phosphate (TTSP) warrant exploration to address persistent interfacial challenges in polyanionic KIB systems.

3.3. Selection of suitable anode material

The successful deployment of KIBs hinges not only on the development of high-performance polyanionic cathodes but critically on the selection and optimization of compatible anode materials capable of efficiently accommodating the large K^+ ion. Carbonaceous materials have been extensively investigated, with graphite being a prominent candidate due to its established intercalation chemistry forming KC_8, offering a theoretical capacity of approximately 279 mAh g^{-1} [95,96]. However, graphite suffers from substantial volumetric expansion (~60 %) during potassiation and often exhibits low initial Coulombic efficiency (ICE) and electrolyte compatibility issues, necessitating strategies such as electrolyte optimization (e.g., ether-based or highly concentrated electrolytes) and advanced binder selection [97,98]. Non-graphitic carbons, including soft and hard carbons, present alternative pathways. Soft carbons, with their more graphitizable nature, can offer improved rate capabilities, while hard carbons, characterized by disordered structures with larger interlayer spacing and intrinsic defects, often demonstrate enhanced cycling stability and a distinct sloping voltage profile followed by a low-potential plateau suitable for K^+ storage [99]. These carbonaceous anodes have shown promise in full cells with polyanionic cathodes like $K_3V_2(PO_4)_2F_3$ and $KFeSO_4F$, primarily due to their relatively stable cycling and appropriate operating potentials, though further improvements in ICE and volumetric energy density are actively pursued.

Beyond carbonaceous systems, potassium metal stands as an ideal anode due to its remarkably high theoretical specific capacity (687 mAh g^{-1}) and the lowest electrochemical potential (2.93 V vs. SHE), which could enable KIBs with maximized energy density when paired with high-voltage polyanionic cathodes [100]. However, its practical application is severely hampered by formidable challenges, including uncontrolled dendrite growth leading to safety hazards, effectively infinite volume changes during plating/stripping cycles, and high chemical reactivity resulting in an unstable SEI. Significant research efforts are directed towards mitigating these issues through strategies like advanced electrolyte formulations, the construction of artificial SEI layers, and the design of 3D current collectors or host frameworks (e.g., porous carbons or potassiophilic substrates) [101–103]. Concurrently, alloy-based anodes (e.g., Sn, Sb, Bi, P) and conversion-type anodes (e.g., metal oxides, sulfides) have garnered attention for their very high theoretical capacities [104]. Nevertheless, these materials typically undergo drastic volumetric changes and structural rearrangements during potassiation/depotassiation, leading to rapid particle pulverization, loss of electrical contact, poor cycling stability, and often significant voltage hysteresis. While nanostructuring and composite formation with conductive carbon can alleviate some of these issues, their long-term stability in full-cell configurations with polyanionic cathodes remains a critical hurdle, despite the theoretical potential for high energy densities [105].

The judicious pairing of anode materials with K-polyanionic cathodes is therefore a complex optimization problem, directly influencing the overall cell voltage, energy density, power density, cycle life, and safety of KIBs. The anode's operating potential, specific capacity, rate capability, and cycling stability must be carefully matched with the characteristics of the polyanionic cathode. Current bottlenecks in KIB technology are significantly tied to anode limitations: for carbon anodes, enhancing ICE, volumetric capacity, and rate performance is crucial; for K-metal, achieving practical safety and long-term reversibility is paramount; and for alloy/conversion anodes, conquering mechanical instability and improving electrochemical reversibility are the primary objectives. Ultimately, advancing KIBs towards practical application necessitates breakthroughs in anode development that can synergistically complement the progress made in high-performance polyanionic cathodes, ensuring stable and efficient electrochemical performance for next-generation energy storage.

4. Visionary perspective

The evolution of KIBs hinges on the rational design of polyanionic cathodes that harmonize high-voltage operation, structural resilience, and sustainable synthesis. While current efforts have established foundational frameworks, transformative breakthroughs will emerge from paradigm-shifting strategies that transcend incremental optimizations. Here, we outline a visionary roadmap addressing three interconnected frontiers: Material genome engineering, Interface-centric system design, and sustainable circular ecosystems, each offering disruptive potential for next-generation KIBs.

4.1. Material genome engineering: beyond trial-and-error discovery

The combinatorial complexity of polyanionic systems (PO_4^{3-}/$P_2O_7^{4-}$/SO_4^{2-}/F^- hybrids) demands a data-driven approach to unlock multi-electron redox couples and metastable phases. Emerging tools in computational thermodynamics and machine learning (ML) can accelerate the discovery of novel K-host frameworks:

(1) Multi-Anion Synergy: Target materials combining inductive (SO_4^{2-}) and inductive-resonance (PO_4^{3-}-F^-) polyanions to amplify redox potentials while maintaining K^+ diffusion kinetics. For instance, Ti-based systems like $KTiPO_4F$, which often suffer from low electronic conductivity, this synergy could be explored by computationally designing structures where secondary anions or strategically placed fluorine not only boost voltage but also favorably alter the Ti 3d orbital overlap or introduce stable Ti^{3+}/Ti^{4+} mixed valency to enhance charge transport. Hypothetical $K_2Fe(SO_4)(PO_4)F$ could leverage synergistic polarization effects to exceed 4.5 V vs. K^+/K.
(2) Dynamic Phase Engineering: Exploit non-equilibrium synthesis (ultrafast sintering, laser ablation) to stabilize high-entropy polyanionic phases (e.g., $K_x(Mn,Fe,V)_2(PO_4)_2(SO_4)F$) with configurational disorder, enabling adaptive volume compensation and potentially creating new conductive pathways in otherwise insulating frameworks.
(3) ML-Guided Screening: Train graph neural networks on existing polyanionic databases to predict stable K^+ migration pathways, voltage profiles, and intrinsic electronic/ionic conductivity. To tackle the low conductivity of materials like $KTiPO_4F$, ML models could be trained with descriptors sensitive to electronic structure (e.g., bond characteristics, coordination environments) to identify novel Ti-based compositions or dopants (e.g., Nb, V) that intrinsically improve electronic conductivity to $>1 \times 10^{-6}$ S cm^{-1} while maintaining structural stability and low strain (<2 %) during potassiation/depotassiation. For fluorophosphates, ML combined with thermodynamic calculations (e.g., DFT-based Pourbaix diagrams for fluorine stability) could screen for compositions or surface modifications that exhibit a higher energy barrier for fluorine extrusion from the lattice under typical KIB operating potentials and temperatures, thus mitigating capacity fade and electrolyte degradation associated with F^- loss.

4.2. Interface-centric system design: breaking the voltage-cyclability trade-off

The instability of high-voltage (>4.3 V) interfaces remains the Achilles' heel of polyanionic cathodes. Future innovations must adopt a hierarchical interface engineering philosophy:

(1) Artificial CEI Layers: Develop atomic-layer-deposited (ALD) or molecular-layer-deposited (MLD) nanoscale coatings (e.g., $LiAlF_4$, $KTaO_3$, conductive polymers) that selectively permit K^+ transport while blocking oxidative solvent decomposition and mitigating anion dissolution. For fluorophosphates prone to fluorine loss, ultra-thin (1–2 nm) F-impermeable coatings like amorphous $KNbO_3$ or $KAlF_4$ could be engineered. These would act as a physical barrier, preventing F^- leaching into the electrolyte and subsequent detrimental reactions, thereby enhancing long-term cycling stability at high voltages. Preliminary work on $LiCoO_2$ suggests <1 nm coatings can reduce capacity fade by 60 % in carbonate electrolytes. ii). iii) Design "smart" electrolytes containing redox-active additives (e.g., TEMPO derivatives, fluorinated cyclic carbonates) that sacrificially electropolymerize at >4.5 V, forming self-healing, ionically conductive CEI layers specifically at the cathode surface, or that can scavenge reactive species resulting from minor fluorine loss.
(2) Solid-State Synergy: Pair polyanionic cathodes with sulfide/thiophosphate solid electrolytes (e.g., K_3PS_4, $K_{10}SnP_2S_{12}$) to eliminate liquid-phase side reactions. Key challenges include mitigating interfacial impedance through tailored Li/K hybrid interlayers or developing cathode-compatible polymer-ceramic composite electrolytes.
(3) Redox-Mediated Electrolytes: Design "smart" electrolytes containing redox-active additives (e.g., (e.g., 2,2,6,6-tetramethylpiperidine nitroxide (TEMPO) derivatives, fluorinated cyclic carbonates) that sacrificially polymerize at >4.5 V, forming self-healing CEI layers specifically at the cathode surface, or that can scavenge reactive species resulting from minor fluorine loss.

4.3. Sustainable circular ecosystems: from lab to gigafactories

The scalability of KIBs hinges on reimagining synthesis and recycling workflows through a closed-loop lens:

(1) Low-Energy Synthesis: Catalyze a shift from energy-intensive solid-state routes (<800 °C) to photochemical/electrochemical methods. For example, UV-assisted sol-gel processes could synthesize $K_3V_2(PO_4)_2F_3$ at 150 °C with 80 % lower carbon footprint. Catalyze a shift from energy-intensive solid-state routes (<800 °C) to photochemical, electrochemical, or low-temperature solvothermal/ionothermal methods. For fluorophosphates, developing synthesis routes like aerosol-assisted deposition or supercritical fluid synthesis at lower temperatures (<300 °C) could minimize fluorine volatilization during material production, improving stoichiometry control and reducing hazardous byproducts. For example, UV-assisted sol-gel processes could synthesize $K_3V_2(PO_4)_2F_3$ at 150 °C with an 80 % lower carbon footprint.
(2) Waste-to-Cathode Valorization: Leverage industrial byproducts (e.g., steel slag-derived $FePO_4$, biomass carbon) as feedstock for polyanionic cathodes, aligning with circular economy principles. Pilot studies show slag-derived $KFePO_4$ achieves 95 % purity at 1/3 the cost of reagent-grade precursors.
(3) Direct Recycling 2.0: Innovate cathode regeneration protocols using deep eutectic solvents (DES) to selectively recover K^+ and transition metals from spent electrodes. Recent advances in DES-based $LiCoO_2$ recycling achieve >99 % metal recovery a template adaptable to $KFeSO_4F$/$KVPO_4F$ systems. Innovate cathode regeneration protocols using advanced techniques like deep eutectic solvents (DES), supercritical fluid extraction, or relithiation/repotassiation strategies to selectively recover K^+ and transition metals, and critically, to reintegrate or stabilize anionic components like fluorine from spent electrodes. For fluorophosphates, DES formulations could be developed that not only dissolve TMs and K salts but also incorporate fluoride salts to maintain fluorine activity, enabling direct resynthesis of the fluorophosphate or recovery of fluorine in a reusable form, adapting principles from $LiCoO_2$ recycling that achieve >99 % metal recovery.

This visionary framework, now augmented with specific material system challenges and targeted research directions, transcends conventional incrementalism, positioning K-polyanionics as enablers of a sustainable energy transition (Fig. 11). By integrating materials innovation with systemic sustainability, the KIB community can redefine the boundaries of electrochemical storage while addressing urgent societal needs.

CRediT authorship contribution statement

Gwangeon Oh: Conceptualization, Data curation, Investigation, Writing – original draft. **Hyokyeong Kang:** Conceptualization,

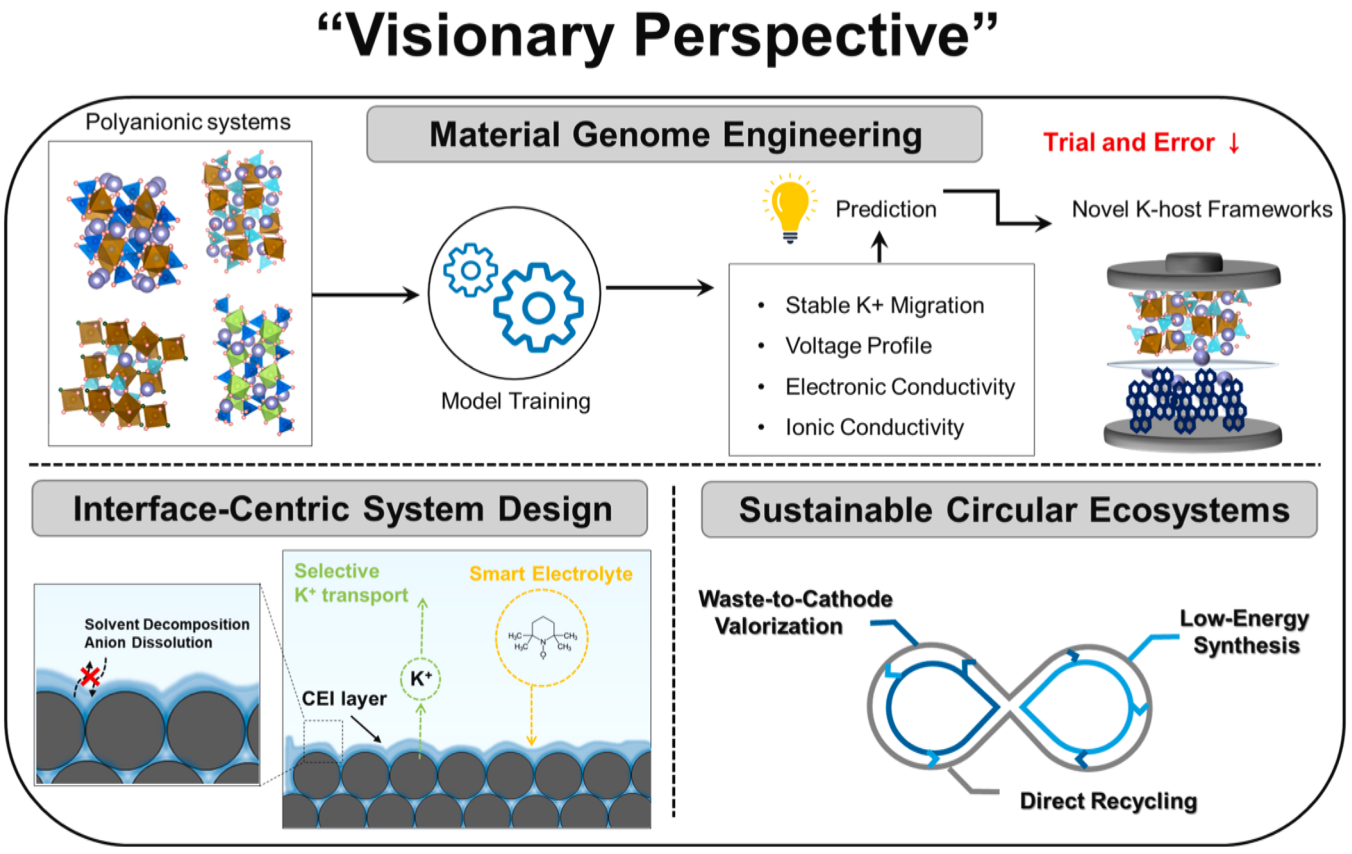

Fig. 11. Schematic illustration of visionary prospects for polyanionic-based cathode materials for KIBs.

Investigation, Writing – original draft. **Hyeona Park:** Conceptualization, Investigation, Writing – original draft. **Heesung Shin:** Investigation, Writing – original draft. **Seungwon Lee:** Investigation, Writing – review & editing. **Changki Jeon:** Investigation, Writing – review & editing. **Shizhao Xiong:** Validation, Writing – review & editing. **Dominic Bresser:** Validation, Writing – review & editing. **Jian Wang:** Data curation, Writing – original draft. **Jang-Yeon Hwang:** Supervision, Conceptualization, Data curation, Investigation, Writing – original draft.

Declaration of competing interest

The authors declare that they have no known competing financial interests or personal relationships that could have appeared to influence the work reported in this paper.

Acknowledgements

This research was supported by the National Research Foundation of Korea (NRF), grant funded by the Korean Government (MSIT) (RS-2024–00408156 and RS-2025–00558312).

References

[1] C.M. Costa, J.C. Barbosa, R. Goncalves, H. Castro, F.J. Del Campo, S. Lanceros-Mendez, Recycling and environmental issues of lithium-ion batteries: advances, challenges and opportunities, Energy Storage Mater. 37 (2021) 433–465, https://doi.org/10.1016/j.ensm.2021.02.032.

[2] S. Chu, Y. Cui, N. Liu, The path towards sustainable energy, Nat. Mater. 16 (2016) 16–22, https://doi.org/10.1038/nmat4834.

[3] Y. Chen, Y. Su, Y. Zhang, Z. Lv, C. Xie, W. Sun, Y. Zhao, M. Xie, Insights into iron-based polyanionic cathodes for scale- energy storage, Energy Storage Mater. 72 (2024) 103722, https://doi.org/10.1016/j.ensm.2024.103722.

[4] K.J. Griffith, K.M. Wiaderek, G. Cibin, L.E. Marbella, C.P. Grey, Niobium tungsten oxides for high–rate lithium–ion energy storage, Nature 559 (2018) 556–563, https://doi.org/10.1038/s41586-018-0347-0.

[5] L. Yan, W. Yang, H. Yu, L. Zhang, J. Shu, Recent progress in rechargeable calcium-ion batteries for high-efficiency energy storage, Energy Storage Mater. (2023) 102822, https://doi.org/10.1016/j.ensm.2023.102822.

[6] H. Liu, H. Du, W. Zhao, X. Qianga, B. Zhenga, Y. Li, B. Cao, Fast potassium migration in mesoporous carbon with ultrathin framework boosting superior rate performance for high-power potassium storage, Energy Storage Mater. 40 (2021) 490–498, https://doi.org/10.1016/j.ensm.2021.05.037.

[7] Y. Xu, Y. Du, H. Chen, J. Chen, T. Ding, D. Sun, D.H. Kim, Z. Lin, X. Zhou, Recent advances in rational design for high-performance potassium-ion batteries, Chem. Soc. Rev. 53 (2024) 7202–7298.

[8] K. Sada, J. Darga, A. Manthiram, Challenges and prospects of sodium-ion and potassium-ion batteries for mass production, Adv. Energy Mater. 13 (2023) 2302321.

[9] X. Ma, H. Fu, J. Shen, D. Zhang, J. Zhou, C. Tong, A.M. Rao, J. Zhou, L. Fan, B. Lu, Green ether electrolytes for sustainable high-voltage potassium ion batteries, Angew. Chemie 135 (2023) e202312973.

[10] J. Li, H. Fu, M. Gu, J. Chen, J. Zhou, L. Fan, B. Lu, Ether-based gel polymer electrolyte for high-voltage potassium ion batteries, Nano Lett. 24 (2024) 11419–11428.

[11] R. Rajagopalan, Y. Tang, X. Ji, C. Jia, H. Wang, Advancements and challenges in potassium ion batteries: a comprehensive review, Adv. Funct. Mater. 30 (2020) 486, https://doi.org/10.1002/adfm.201909486, 1909.

[12] Y. Xu, Y. Du, H. Chen, J. Chen, T. Ding, D. Sun, D.H. Kim, Z. Lin, X. Zhou, Recent advances in rational design for high–performance potassium–ion batteries, Chem. Soc. Rev. 53 (2024) 7202–7298, https://doi.org/10.1039/D3CS00601H.

[13] J. Wang, F. Liu, G. Qin, X. He, Conformational gearing of black phosphorus anode via biomimetic adaptive mechanism for fast charging and low-temperature adaptability in potassium batteries, Energy Storage Mater. 76 (2025) 104101, https://doi.org/10.1016/j.ensm.2025.104101.

[14] J.–Y. Hwang, J. Kim, T.–Y. Yu, S.–T. Myung, Y.–K. Sun, Development of P3–$K_{0.69}CrO_2$ as an ultra–high–performance cathode material for K–ion batteries, Energy Environ. Sci. 11 (2018) 2821–2827, https://doi.org/10.1039/C8EE01365A.

[15] Y. Gao, Q. Yu, H. Yang, J. Zhang, W. Wang, The enormous potential of sodium/potassium-ion batteries as the mainstream energy storage technology for large-scale commercial applications, Adv. Mater. 36 (2024) 2405989, https://doi.org/10.1002/adma.202405989.

[16] T. Hosaka, K. Kubota, A.S. Hameed, S. Komaba, Research development on K–ion batteries, Chem. Rev. 120 (2020) 6358–6466, https://doi.org/10.1021/acs.chemrev.9b00463.

[17] B. Ji, W. Yao, Y. Zheng, P. Kidkhunthod, X. Zhou, S. Tunmee, S. Sattayaporn, H.-M. Cheng, H. He, Y. Tang, A fluoroxalate cathode material for potassium-ion

batteries with ultra-long cyclability, Nat. Commun. 11 (2020) 1225, https://doi.org/10.1038/s41467-020-15044-y.
[18] H. Chen, L.–K. Zhao, X. Cheng, X.–W. Gao, Z. Liu, S.–D. Li, D.–R. Yang, T.–Z. Ren, W.–B. Luo, Boosting structural stability and air stability towards layered oxide cathodes for potassium ion batteries, Chem. Eng. J. 507 (2025) 160252, https://doi.org/10.1016/j.cej.2025.160252.
[19] W. Shu, C. Han, X. Wang, Prussian blue analogues cathodes for nonaqueous potassium–ion batteries: past, present, and future, Adv. Funct. Mater. 34 (2024) 2309636, https://doi.org/10.1002/adfm.202309636.
[20] K.–Y. Zhang, Z.–Y. Gu, E.H. Ang, J.Z. Guo, X.T. Wang, Y. Wang, X.–L. Wu, Advanced polyanionic electrode materials for potassium–ion batteries: progresses, challenges and application prospects, Mater. Today 54 (2022) 189–201, https://doi.org/10.1016/j.mattod.2022.02.01.
[21] C. Xu, J. Zhao, C. Yang, Y.-S. Hu, Polyanionic cathode materials for practical Na-ion batteries toward high energy density and long cycle life, ACS. Cent. Sci. 9 (2023) 1721–1736, https://doi.org/10.1021/acscentsci.3c00907.
[22] K.-Y. Zhang, Z.-Y. Gu, E.H. Ang, J.-Z. Guo, X.-T. Wang, Y. Wang, X.-L. Wu, Advanced polyanionic electrode materials for potassium-ion batteries: progresses, challenges and application prospects, Mater. Today 54 (2022) 189–201, https://doi.org/10.1016/j.mattod.2022.02.013.
[23] X. Zhang, D. Yang, X. Rui, Y. Yu, S. Huang, Advanced cathodes for potassium-ion battery, Curr. Opin. Electrochem. 18 (2019) 24–30, https://doi.org/10.1039/D0TA12129K.
[24] G. Chen, Q. Huang, T. Wu, L. Lu, Polyanion Sodium Vnadium Phosphate for Next Generation of Sodium-Ion Batteries-A Review, Adv. Funct. Mater. 30 (2020) 2001289, https://doi.org/10.1002/adfm.202001289.
[25] B. Senthilkumar, C. Murugesan, L. Sharma, S. Lochab, P. Barpanda, An overview of mixed polyanionic cathode materials for sodium–ion batteries, Small. Methods 3 (2019) 1800253, https://doi.org/10.1002/smtd.201800253.
[26] Y. Lan, W. Yao, X. He, T. Song, Y. Tang, Mixed polyanionic compounds as positive electrodes for low–cost electrochemical energy storage, Angew. Chemie Int. Ed. 59 (2020) 9255–9262, https://doi.org/10.1002/anie.201915666.
[27] H. Park, H. Kim, W. Ko, J.H. Jo, Y. Lee, J. Kang, I. Park, S.–T. Myung, J. Kim, Development of $K_4Fe_3(PO_4)_2(P_2O_7)$ as a novel Fe–based cathode with high energy densities and excellent cyclability in rechargeable potassium batteries, Energy Storage Mater. 28 (2020) 47–54, https://doi.org/10.1016/j.ensm.2020.02.031.
[28] X. Lin, J. Huang, H. Tan, J. Huang, B. Zhang, $K_3V_2(PO_4)_2F_3$ as a robust cathode for potassium–ion batteries, Energy Storage Mater. 16 (2019) 97–101, https://doi.org/10.1016/j.ensm.2018.04.026.
[29] T. Song, W. Yao, P. Kiadkhunthod, Y. Zheng, N. Wu, X. Zhou, S. Tunmee, S. Sattayaporn, Y. Tang, A low–cost and environmentally friendly mixed polyanionic cathode for sodium–ion storage, Angew. Chemie 132 (2020) 750–755, https://doi.org/10.1002/ange.201912272.
[30] Y.-W. Byeon, M.-J. Gong, Z. Cai, Y. Sun, N.J. Szymanski, J. Bai, D.-H. Seo, H. Kim, Effects of cation and anion substitution in $KVPO_4F$ for K-ion batteries, Energy Storage Mater. 57 (2023) 81–91, https://doi.org/10.1016/j.ensm.2023.02.007.
[31] H. Liu, J. Xu, Y. Xu, Z. Yuan, L. Duan, Y. Lv, J. Liao, J. Bao, X. Zhou, Suppressing fluorine loss of $KVPO_4F$ by surface chromium substitution for high-efficiency potassium-ion batteries, Energy Storage Mater. 75 (2025) 104017.
[32] J.–Y. Hwang, S.–T. Myung, Y.–K. Sun, Sodium–ion batteries: present and future, Chem. Soc. Rev. 46 (2017) 3529–3614, https://doi.org/10.1039/C6CS00776G.
[33] X. Zhang, B. Wang, S. Zhao, H. Li, H. Yu, Oxygen anionic redox activated high-energy cathodes: status and prospects, Etransportation 8 (2021) 100118, https://doi.org/10.1016/j.etran.2021.100118.
[34] J. Wang, B. Ouyang, H. Kim, Y. Tian, G. Ceder, H. Kim, Computational and experimental search for potential polyanionic K-ion cathode materials, J. Mater. Chem. A 9 (2021) 18564–18575, https://doi.org/10.1039/D1TA05300K.
[35] H. Rostami, J. Valio, P. Suominen, P. Tynjälä, U. Lassi, Advancements in cathode technology, recycling strategies, and market dynamics: a comprehensive review of sodium ion batteries, Chem. Eng. J. 495 (2024) 153471, https://doi.org/10.1016/j.cej.2024.153471.
[36] M.G.T. Nathan, H. Yu, G.–T. Kim, J.–H. Kim, J.S. Cho, J. Kim, J.–K. Kim, Recent advances in layered metal–oxide cathodes for application in potassium–ion batteries, Adv. Sci. 9 (2022) 2105882, https://doi.org/10.1002/advs.202105882.
[37] H. Liu, J. Xu, Y. Xu, Z. Yuan, L. Duan, Y. Lv, J. Liao, J. Bao, X. Zhou, Suppressing fluorine loss of $KVPO_4F$ by surface chromium substitution for high–efficiency potassium–ion batteries, Energy Storage Mater. 75 (2025) 104017, https://doi.org/10.1016/j.ensm.2025.104017.
[38] J. Gu, L. He, X. Wang, X. Ge, W. Zhou, C. Guan, Z. Zhang, Tuning TM-O bond covalency to boost cationic activity and reversibility of $Na_4Fe_{1.5}Mn_{1.5}(PO_4)_2P_2O_7$, Nano Lett. 25 (2025) 7826–7834, https://doi.org/10.1021/acs.nanolett.5c00931.
[39] Y. Liu, W. Li, Y. Xia, Recent progress in polyanionic anode materials for Li (Na)–ion batteries, Electrochem. Energy Rev. 4 (2021) 447–472, https://doi.org/10.1007/s41918-021-00095-6.
[40] T. Jin, H. Li, K. Zhu, P.–F. Wang, P. Liu, L. Jiao, Polyanion–type cathode materials for sodium–ion batteries, Chem. Soc. Rev. 49 (2020), https://doi.org/10.1039/C9CS00846B, 2342-F 2377.
[41] N. Recham, G. Rousse, M.T. Sougrati, J.N. Chotard, C. Frayret, S. Mariyappan, B. C. Melot, J.C. Jumas, J.M. Tarascon, Preparation and characterization of a stable $FeSO_4F$–based framework for alkali ion insertion electrodes, Chem. Mater. 24 (2012) 4363–4370, https://doi.org/10.1021/cm302428w.
[42] V. Mathew, S. Kim, J. Kang, J. Gim, J. Song, J. Baboo, W. Park, D. Ahn, J. Han, L. Gu, Y. Wang, Y.–S. Hu, Y.–K. Sun, J. Kim, Amorphous iron phosphate: potential host for various charge carrier ions, NPG Asia Mater. 6 (2014) e138, https://doi.org/10.1038/am.2014.98.
[43] J. Han, G.–N. Li, F. Liu, M. Wang, Y. Zhang, L. Hu, C. Dai, M. Xu, Investigation of $K_3V_2(PO_4)_3$/C nanocomposites as high potential cathode materials for potassium–ion batteries, Chem. Commun. 53 (2017) 1805–1808, https://doi.org/10.1039/C6CC10065A.
[44] K. Chihara, A. Katogi, K. Kubota, S. Komaba, $KVPO_4F$ and $KVOPO_4$ toward 4 V–class potassium–ion batteries, Chem. Commun. 53 (2017) 5208–5211, https://doi.org/10.1039/C6CC10280H.
[45] J. Kang, W. Ko, H. Park, Y. Lee, J.H. Jo, J.U. Choi, S.–T. Myung, J. Kim, High power rhombohedral $Fe_2(SO_4)_3$ with outstanding cycle performance as Fe based cathode for K–ion batteries, Energy Storage Mater. 33 (2020) 276–282, https://doi.org/10.1016/j.ensm.2020.08.024.
[46] L. Liu, J. Su, X. Zhou, D. Liang, Y. Liu, R. Tang, Y. Xu, Y. Jiang, Z. Wei, Conductivity versus structure dependence investigation of $Na_{1+x}Zr_2Si_xP_{3-x}O_{12}$ ($0 \leq x \leq 3$) through composition optimization by adjusting Si/P ratio, Mater. Today Chem. 30 (2023) 101495, https://doi.org/10.1016/j.mtchem.2023.101495.
[47] F. Lalère, V. Seznec, M. Courty, R. David, J.N. Chotard, C. Masquelier, Improving the energy density of $Na_3V_2(PO_4)_3$ based positive electrodes through V/Al substitution, J. Mater. Chem. A 3 (2015) 16198–16205, https://doi.org/10.1039/C5TA03528G.
[48] X. Wang, C. Niu, J. Meng, P. Hu, X. Xu, X. Wei, L. Zhou, K. Zhao, W. Luo, M. Yan, L. Mai, Novel $K_3V_2(PO_4)_3$/C bundled nanowires as superior sodium-ion battery electrode with ultrahigh cycling stability, Adv. Energy Mater. 5 (2015) 1500716, https://doi.org/10.1002/aenm.201500716.
[49] M. Ragupathi, R.K. Selvan, K–ion intercalation behavior of carbon–coated $K_3V_2(PO_4)_3$ nanostructures prepared by the sol–gel method, Ceram. Int. 50 (2024) 14490–14496, https://doi.org/10.1016/j.ceramint.2024.01.361.
[50] R.–J. Luo, C.–Y. Du, C. Ma, J. Zeng, X. Xu, Z. Qian, Z. Mei, Z.–T. Zhou, Z.–Y. Zhu, Y.–N. Zhou, Orthorhombic $K_3V_3(PO_4)_4$: a low–temperature cathode material for potassium–ion batteries, Chem. Eng. J. 491 (2024) 151968, https://doi.org/10.1016/j.cej.2024.151968.
[51] X. Zhang, X. Kuang, H. Zhu, N. Xiao, Q. Zhang, X. Rui, Y. Yu, S. Huang, Hybrid cathodes composed of $K_3V_2(PO_4)_3$ and carbon materials with boosted charge transfer for K–ion batteries, Surfaces 3 (2020) 1–10, https://doi.org/10.3390/surfaces3010001.
[52] S. Zheng, S. Cheng, S. Xiao, L. Hu, Z. Chen, B. Huang, Q. Liu, J. Yang, Q. Chen, Partial replacement of K by Rb to improve electrochemical performance of $K_3V_2(PO_4)_3$ cathode material for potassium–ion batteries, J. Alloys. Compd. 815 (2020) 152379, https://doi.org/10.1016/j.jallcom.2019.152379.
[53] J. Bodart, N. Eshraghi, T. Carabin, B. Vertruyen, R. Cloots, F. Boschini, A. Mahmoud, Spray–dried $K_3V(PO_4)_2$/C composites as novel cathode materials for K–ion batteries with superior electrochemical performance, J. Power. Sources. 480 (2020) 229057, https://doi.org/10.1016/j.jpowsour.2020.229057.
[54] L. Zhang, B. Zhang, C. Wang, Y. Dou, Q. Zhang, Y. Liu, H. Gao, M. Al–Mamun, W. K. Pang, Z. Guo, S.X. Dou, H.K. Liu, Constructing the best symmetric full K–ion battery with the NASICON–type $K_3V_2(PO_4)$, Nano Energy 60 (2019) 432–439, https://doi.org/10.1016/j.nanoen.2019.03.085.
[55] N. Voronina, J.H. Jo, A. Konarov, J. Kim, S. Myung, $KTi_2(PO_4)_3$ electrode with a long cycling stability for potassium–ion batteries, Small. 16 (2020) 2001090.
[56] J. Dong, J. Xiao, K. Cao, H. He, Y. Zhu, H. Liu, C. Chen, Encapsulation of $KTi_2(PO_4)_3$ nanoparticles in porous N–doped carbon nanofibers as a free standing electrode for superior Na/K–storage performance, J. Alloys. Compd. 937 (2023) 168358, https://doi.org/10.1016/j.jallcom.2022.168358.
[57] L. Zhang, X. Fang, M. Ou, Y. Chen, J. Xu, X. Gu, X. Zhao, Selective phosphorylation of MOF to construct KTP/KTOP/C heterojunction for high performance potassium–ion batteries, Appl. Surf. Sci. 652 (2024) 159290, https://doi.org/10.1016/j.apsusc.2024.159290.
[58] S. Liu, X. Li, S. Zhong, W. Jiang, Y. Liu, W. Ding, H. Hu, Z. Huang, L. Liu, Electrosprayed hierarchical mesoporous $Mn_{0.5}Ti_2(PO_4)_3$@C microspheres as promising high–performance anode for potassium–ion batteries, J. Colloid. Interface Sci. 658 (2024) 923–933, https://doi.org/10.1016/j.jcis.2023.12.122.
[59] J. Dai, D. Su, J. Yang, W. Zhang, Q. Wang, L. Liu, H. Hu, H. Li, Z. Liu, A flexible $Mn_{0.5}Ti_2(PO_4)_3$/C nanofiber film with superior cycling stability for potassium–ion batteries, Nanoscale 13 (2021) 19956–19965, https://doi.org/10.1039/D1NR04735C.
[60] J. Li, Y. Zheng, K. San Hui, K. Wang, C. Zha, D.A. Dinh, J. Tu, Z. Shao, K.N. Hui, Enhanced K–storage performance in ultralong cycle life potassium–ion batteries achieved via carbothermal–reduction–synthesized $KVOPO_4$ cathode, Energy Stor. Mater. 61 (2023) 102852, https://doi.org/10.1016/j.ensm.2023.102852.
[61] R. Lian, D. Wang, X. Ming, R. Zhang, Y. Wei, J. Feng, X. Meng, G. Chen, Phase transformation, ionic diffusion, and charge transfer mechanisms of $KVOPO_4$ in potassium ion batteries: first–principles calculations, J. Mater. Chem. A 6 (2018) 16228–16234, https://doi.org/10.1039/C8TA06708B.
[62] Y. Qi, J. Li, W. Zhong, S. Bao, M. Xu, $KTiOPO_4$: a long–life, high–rate and low–temperature–workable host for Na/K–ion batteries, Chem. Eng. J. 417 (2021) 128159, https://doi.org/10.1016/j.cej.2020.128159.
[63] P.R. Kumar, K. Kubota, D. Igarashi, S. Komaba, Enhanced electrochemical properties of $KTiOPO_4$–rGO negative electrode for sodium and potassium ion batteries, J. Phys. Chem. C 125 (2021) 24823–24830, https://doi.org/10.1021/acs.jpcc.1c08339.
[64] J. Huang, X. Cai, H. Yin, Y. Li, W. Lin, S. Huang, Y. Zhang, A new candidate in polyanionic compounds for a potassium–ion battery cathode: $kTiOPO_4$, J. Phys. Chem. Lett. 12 (2021) 2721–2726, https://doi.org/10.1021/acs.jpclett.1c00286.
[65] S.S. Fedotov, N.D. Luchinin, D.A. Aksyonov, A.V. Morozov, S.V. Ryazantsev, M. Gaboardi, J.R. Plaisier, K.J. Stevenson, A.M. Abakumov, E.V. Antipov, Titanium–based potassium–ion battery positive electrode with extraordinarily

high redox potential, Nat. Commun. 11 (2020) 1484, https://doi.org/10.1038/s41467-020-15244-6.
[66] H. Kim, D.H. Seo, M. Bianchini, R.J. Clément, H. Kim, J.C. Kim, Y. Tian, T. Shi, W. S. Yoon, G. Ceder, A new strategy for high–voltage cathodes for K–ion batteries: toichiometric $KVPO_4F$, Adv. Energy Mater. 8 (2018) 1801591, https://doi.org/10.1002/aenm.201801591.
[67] Z. Liu, J. Wang, B. Lu, Plum pudding model inspired $KVPO_4F$@3DC as high–voltage and hyperstable cathode for potassium ion batteries, Sci. Bull. 65 (2020) 1241–1251, https://doi.org/10.1016/j.scib.2020.04.010.
[68] C. Xie, X. Liu, J. Han, L. Lv, X. Zhou, C. Han, Y. You, Pomegranate–like $KVPO_4F$@C microspheres as high volumetric energy density cathode for potassium–ion batteries, Small. 18 (2022) 2204348, https://doi.org/10.1002/smll.202204348.
[69] J. Liao, X. Zhang, Q. Zhang, Q. Hu, Y. Li, Y. Du, J. Xu, L. Gu, X. Zhou, Synthesis of $KVPO_4F$/carbon porous single crystalline nanoplates for high rate potassium–ion batteries, Nano Lett. 22 (2022) 4933–4940, https://doi.org/10.1021/acs.nanolett.2c01604.
[70] Y. Heng, Z. Gu, J. Guo, H. Liang, Y. Liu, W. Guo, X. Zhao, X. Wang, X. Wu, Low strain and high energy $KVPO_4F$ cathode with multifunctional stabilizer for advanced potassium–ion batteries, Energy Environ. Mater. 7 (2024) e12721, https://doi.org/10.1002/eem2.12721.
[71] J. Zhao, Y. Qin, L. Li, H. Wu, X. Jia, X. Zhu, H. Zhao, Y. Su, S. Ding, Pillar strategy enhanced ion transport and structural stability toward ultra stable $KVPO_4F$ cathode for practical potassium–ion batteries, Sci. Bull. 68 (2023) 593–602, https://doi.org/10.1016/j.scib.2023.02.029.
[72] Y. Zhu, B. Ou, C. Gao, Y. Gao, B. Zhang, F. Kang, D. Zhai, Ligand engineering enables fast kinetics of $KVPO_4F$ cathode for potassium–ion batteries, ACS. Energy Lett. 9 (2024) 3212–3218, https://doi.org/10.1021/acsenergylett.4c01052.
[73] V. Ramezankhani, N.D. Luchinin, S.N. Marshenya, M.V. Zakharkin, A. A. Golubnichiy, A.V. Morozov, O. Emilianova, K.J. Stevenson, E.V. Antipov, A. M. Abakumov, Exploring $KTiPO_4F$ as a robust polyanion anode material for potassium–ion batteries, J. Mater. Chem. A 12 (2024) 18404–18411, https://doi.org/10.1039/D3TA08103F.
[74] W.B. Park, S.C. Han, C. Park, S.U. Hong, U. Han, S.P. Singh, Y.H. Jung, D. Ahn, K.–.S. Sohn, M. Pyo, KVP_2O_7 as a robust high–energy cathode for potassium–ion batteries: pinpointed by a full screening of the inorganic registry under specific search conditions, Adv. Energy Mater. 8 (2018) 1703099, https://doi.org/10.1002/aenm.201703099.
[75] H. Park, H. Kim, W. Ko, J.H. Jo, Y. Lee, J. Kang, I. Park, S.–T. Myung, J. Kim, Development of $K_4Fe_3(PO_4)_2(P_2O_7)$ as a novel Fe–based cathode with high energy densities and excellent cyclability in rechargeable potassium batteries, Energy Stor. Mater. 28 (2020) 47–54.
[76] B. Senthilkumar, C. Murugesan, K. Sada, P. Barpanda, Electrochemical insertion of potassium ions in $Na_4Fe_3(PO_4)_2P_2O_7$ mixed phosphate, J. Power. Sources. 480 (2020) 228794, https://doi.org/10.1016/j.jpowsour.2020.228794.
[77] J. Kang, H. Park, W. Ko, Y. Lee, J. Ahn, J.–.K. Yoo, S.H. Song, H. Kim, J. Kim, Low–cost and high–power $K_4[Mn_2Fe](PO_4)_2(P_2O_7)$ as a novel cathode with outstanding cyclability for K–ion batteries, J. Mater. Chem. A 9 (2021) 9898–9908, https://doi.org/10.1039/D1TA01602D.
[78] W. Ko, H. Park, J.H. Jo, Y. Lee, J. Kang, Y.H. Jung, T.Y. Jeon, S.T. Myung, J. Kim, Unveiling yavapaiite–type $K_xFe(SO_4)_2$ as a new Fe–based cathode with outstanding electrochemical performance for potassium–ion batteries, Nano Energy 66 (2019) 104184, https://doi.org/10.1016/j.nanoen.2019.104184.
[79] P.R. Kumar, T. Hosaka, T. Shimamura, D. Igarashi, S. Komaba, Mg–Doped $KFeSO_4F$ as a high–performance cathode material for potassium–ion batteries, ACS. Appl. Energy Mater. 5 (2022) 13470–13479, https://doi.org/10.1021/acsaem.2c02148.
[80] J. Liao, Q. Hu, Y. Du, J. Li, L. Duan, J. Bao, X. Zhou, Robust carbon nanotube–interwoven $KFeSO_4F$ microspheres as reliable potassium cathodes, Sci. Bull. 67 (2022) 2208–2215, https://doi.org/10.1016/j.scib.2022.10.012.
[81] H. Kim, Y. Tian, G. Ceder, Origin of capacity degradation of high–voltage $KVPO_4F$ cathode, J. Electrochem. Soc. 167 (2020) 110555, https://doi.org/10.1149/1945-7111/aba54e.
[82] Z. Zhang, R. Wang, Z. Chen, X. Liu, Z. Liu, J. Zeng, X. Zhao, K. Peng, Q. Yao, X. Zhang, K. Shi, C. Zhu, X. Yan, A micron-size carbon-free $K_3V_2O_2(PO_4)_2F$ cathode with high-rate performance for potassium-ion batteries, J. Chem. Eng. 436 (2022) 135235.
[83] H. He, J. Si, S. Zeng, N. Ren, H. Liu, C.-H. Chen, Vanadium-based pyrophosphate material $K_2(VO)_3(P_2O_7)_2$ as a high voltage cathode for potassium ion batteries, ACS. Appl. Energy Mater. 7 (2024) 41–47.
[84] H. He, K. Cao, S. Zeng, J. Si, Y. Zhu, C.-H. Chen, $K_2VOP_2O_7$ as a novel high-voltage cathode material for potassium ion batteries, J. Power. Sources. 587 (2023) 233715, https://doi.org/10.1016/j.jpowsour.2023.233715.
[85] F. Wang, S. Liu, Q. Jiang, K. Feng, X. Yang, X. Li, H. Zhang, M. Xia, H. Zhang, $K_2Fe_3(SO_4)_3(OH)_2(H_2O)_2$: a new high-performance hydroxysulfate cathode material for alkali metal ion batteries, J. Power. Sources. 452 (2020) 227835, https://doi.org/10.1016/j.jpowsour.2020.227835.
[86] W. Wang, B. Ji, W. Yao, X. Zhang, Y. Zheng, X. Zhou, P. Kidkhunthod, H. He, Y. Tang, A novel low-cost and environment-friendly cathode with large channels and high structure stability for potassium-ion storage, Sci. China Mater. 64 (2021) 1047–1057, https://doi.org/10.1007/s40843-020-1512-0.
[87] W. Deriouche, E. Anger, M. Freire, A. Maignan, N. Amdouni, V. Pralong, A vanadium oxy-phosphate $Na_4VO(PO_4)_2$ as cathode material for Na ion batteries, Solid. State Sci. 72 (2017) 124–129, https://doi.org/10.1016/j.solidstatesciences.2017.08.017.
[88] R. Muruganantham, Y.-T. Chiu, C.-C. Yang, C.-W. Wang, W.-R. Liu, An efficient evaluation of F-doped polyanion cathode materials with long cycle life for Na-ion batteries applications, Sci. Rep. 7 (2017) 14808, https://doi.org/10.1038/s41598-017-13718-0.
[89] Z.-Y. Gu, X.-T. Wang, Y.-L. Heng, Y. Liu, S.-H. Zheng, K.-Y. Zhang, Z.-L. Hao, X.-L. Wu, Polyanionic cathodes for sodium-ion batteries: materials, working mechanism, and applications, Mater. Sci. Eng. R: Rep. 165 (2025) 101008, https://doi.org/10.1016/j.mser.2025.101008.
[90] X. Xiao, Y. Lan, L. Tan, H. Xu, W. Yao, Y. Tang, Alluaudite $Na_2Fe_2(SO_4)_3$ and NASICON-Type $Na_4Fe_3(PO_4)_2(P_2O_7)$ as promising cathode materials in sodium-ion batteries, Adv. Funct. Mater. 34 (2024) 2411280, https://doi.org/10.1002/adfm.202411280.
[91] Z. Lv, M. Ling, M. Yue, X. Li, M. Song, Q. Zheng, H. Zhang, Vanadium-based polyanionic compounds as cathode materials for sodium-ion batteries: toward high-energy and high-power applications, J. Energy Chem. 55 (2021) 361–390, https://doi.org/10.1016/j.jechem.2020.07.008.
[92] R.R. Samigullin, Z.V. Bobyleva, M.V. Zakharkin, E.V. Zharikova, M.G. Rozova, O. A. Drozhzhin, E.V. Antipov, On the thermal stability of selected electrode materials and electrolytes for Na–ion batteries, Energies (Basel) 17 (2024) 3970, https://doi.org/10.3390/en17163970.
[93] J. Liao, Q. Hu, B. Che, X. Ding, F. Chen, C. Chen, Competing with other polyanionic cathode materials for potassium–ion batteries via fine structure design: new layered $KVOPO_4$ with a tailored particle morphology, J. Mater. Chem. A 7 (2019) 15244–15251, https://doi.org/10.1039/C9TA03192H.
[94] N.S. Katorova, D.P. Rupasov, S.S. Fedotov, N.D. Luchinin, A.M. Abakumov, K. J. Stevenson, In Electrochemical Society Meeting Abstracts ecee2019, The Electrochemical Society, Inc., 2019, p. 257, https://doi.org/10.1149/MA2019-04/5/257.
[95] Y. Yan, J. Hu, Y. Gao, T. Hou, B. Zhang, J. Liang, B. Li, F. Kang, D. Zhai, Unveiling the influence of dehydrofluorination of poly (vinylidene fluoride) binder on the failure of graphite anode in potassium-ion batteries, Angew. Chemie Int. Ed. (2025) e202502872.
[96] X. Li, J. Li, L. Ma, C. Yu, Z. Ji, L. Pan, W. Mai, Graphite anode for potassium ion batteries: current status and perspective, Energy Environ. Mater. 5 (2022) 458–469.
[97] F. Yuan, J. Hu, Y. Lei, R. Zhao, C. Gao, H. Wang, B. Li, F. Kang, D. Zhai, Key factor determining the cyclic stability of the graphite anode in potassium-ion batteries, ACS. Nano 16 (2022) 12511–12519.
[98] W. Zhou, Y. Mo, P. Gao, K. Wang, J. Ke, Z. Liu, S. Chen, J. Liu, Decoupling interfacial kinetics realizes 5C fast charging of potassium-ion batteries using graphite anode, Adv. Funct. Mater. 34 (2024) 2312994, https://doi.org/10.1002/adfm.202312994.
[99] S. Wu, Y. Song, C. Lu, T. Yang, S. Yuan, X. Tian, Z. Liu, High-rate soft carbon anode in potassium ion batteries: the role of chemical structures of pitches, Carbon. N. Y. 203 (2023) 211–220, https://doi.org/10.1016/j.carbon.2022.11.058.
[100] Y. Feng, A.M. Rao, J. Zhou, B. Lu, Selective potassium deposition enables dendrite-resistant anodes for ultrastable potassium-metal batteries, Adv. Mater. 35 (2023) 2300886, https://doi.org/10.1002/adma.202300886.
[101] Z. Wei, A. Wang, X. Guan, G. Li, Z. Yang, C. Huang, J. Zhang, L. Ren, J. Luo, X. Liu, Processable potassium metal anode for stable batteries, Energy Environ. Mater. 5 (2022) 1278–1284, https://doi.org/10.1002/eem2.12244.
[102] F. Yang, J. Hao, J. Long, S. Liu, T. Zheng, W. Lie, J. Chen, Z. Guo, Achieving high-performance metal phosphide anode for potassium ion batteries via concentrated electrolyte chemistry, Adv. Energy Mater. 11 (2021) 2003346, https://doi.org/10.1002/aenm.202003346Ci.
[103] S. Li, H. Zhu, Y. Liu, Z. Han, L. Peng, S. Li, C. Yu, S. Cheng, J. Xie, Codoped porous carbon nanofibres as a potassium metal host for nonaqueous K-ion batteries, Nat. Commun. 13 (2022) 4911, https://doi.org/10.1038/s41467-022-32660-y.
[104] X. Wang, S. Tang, W. Guo, Y. Fu, A. Manthiram, Advances in multimetallic alloy-based anodes for alkali-ion and alkali-metal batteries, Mater. Today 50 (2021) 259–275, https://doi.org/10.1016/j.mattod.2021.05.001.
[105] Q. Wu, B. Chen, H. Xie, X. Bai, M. Liang, Z. Wu, X. Jin, C. He, N. Zhao, Bismuth-antimony alloy nanoparticles encapsulated in 3D carbon framework: synergistic effect for enhancing interfacial potassium storage, Chem. Eng. J. 430 (2022) 132906, https://doi.org/10.1016/j.cej.2021.132906.